Flexible and Printed Electronics

Challenges and opportunities in upscaling inkjet-printing of OPV

IOP Publishing Flex. Print. Electron. 9 (2024) 043001 https://doi.org/10.1088/2058-8585/ad7ece

Flexible and Printed Electronics

TOPICAL REVIEW

Challenges and opportunities in upscaling inkjet-printing of OPV

Marc Steinberger[1,*], Qingguang Xie[2], Olivier J J Ronsin[2], Philipp Maisch[1], Kai Cheong Tam[1], Andreas Distler[1], Jens Harting[2,3], Christoph J Brabec[1,4,*] and Hans-Joachim Egelhaaf[1,4]

[1] Institute of Materials for Electronics and Energy Technology (i-MEET), Friedrich-Alexander-Universität Erlangen-Nürnberg, Martensstr. 7, 91058 Erlangen, Germany
[2] Helmholtz Institute Erlangen-Nürnberg for Renewable Energy (HI ERN), Forschungszentrum Jülich, Cauerstr. 1, D-91058 Erlangen, Germany
[3] Department of Chemical and Biological Engineering and Department of Physics, Friedrich-Alexander-Universität Erlangen-Nürnberg, Cauerstr. 1, D-91058 Erlangen, Germany
[4] Helmholtz-Institute Erlangen-Nürnberg for Renewable Energy (HI ERN), Immerwahrstraße 2, 91058 Erlangen, Germany
[*] Authors to whom any correspondence should be addressed.

E-mail: marc.steinberger@fau.de and christoph.brabec@fau.de

Keywords: inkjet-printing, organic photovoltaics, upscaling

OPEN ACCESS

RECEIVED
9 February 2024

REVISED
16 August 2024

ACCEPTED FOR PUBLICATION
24 September 2024

PUBLISHED
29 October 2024

Abstract

The power conversion efficiency and long-term stability of organic solar cells have increased tremendously over the past years, reaching up to 19.2% on research cells and 14.5% on large modules. To take the final step towards industrialization, fabrication methods that can be upscaled and directly implemented in industrial processes need to be developed. In recent years, well-known industrial techniques, like drop-on-demand inkjet printing, have been further developed within the organic photovoltaics (OPV) community, as it enables versatile printing of arbitrary, free-form organic solar modules with different colors-a key feature for modern building-integrated photovoltaics and several niche applications of OPV printed on any kind object. In this review, aside a brief summary of recent developments, we provide an overview of the biggest challenges in OPV inkjet-printing and define design rules to overcome these issues. Further perspectives of OPV inkjet-printing conclude the review.

1. Principles and state of the art of printed photovoltaics (PV)

The energy demand of the growing world population is tremendous and rising. In 2022, the primary energy consumption amounted to around 179 000 TWh [1]. Although solar power is one of the cheapest and most sustainable pathways to meet these demands, it contributed as little as 3400 TWh, i.e. less than 2%. Notwithstanding that the number of PV installations is growing rapidly, further growth in densely populated areas is limited by the lack of space, while the conversion of agricultural areas for solar power plants is not a sustainable solution and transport over larger distances is costly. Energizing existing surfaces, e.g. facades and rooftops, will therefore be a solution to generating electricity where it is needed, i.e. in the big cities (figure 1). The combination of PV installations with agriculture will allow dual use of land. Off-grid PV installations, although not contributing substantially to electricity generation on a global scale, can provide economic solutions in many applications, ranging from the powering of internet-of-things (IoT) devices to charging mobile phones in regions with wide-mesh electricity infrastructure.

Printed PV, especially organic photovoltaics (OPV), is ideally suited for integration in a vast number of applications (figure 1), as it combines unique traits, such as (ultra-)light weight, flexibility, semitransparency, and discretionary shapes and colors, which are not readily provided by silicon PV [4].

1.1. Printed OPV-recent advances and future challenges in cells and modules

The OPV technology does not only meet the above-mentioned requirements for 'integration into anything', but it also has shown tremendous development of power conversion efficiencies (PCE's) in recent years as shown in figure 2 [5–7].

Due to the development of novel materials, mainly of the donor and acceptor components of the active layer, certified PCE's have been rocketing since 2018, reaching 19.2% in 2023 on the research cell

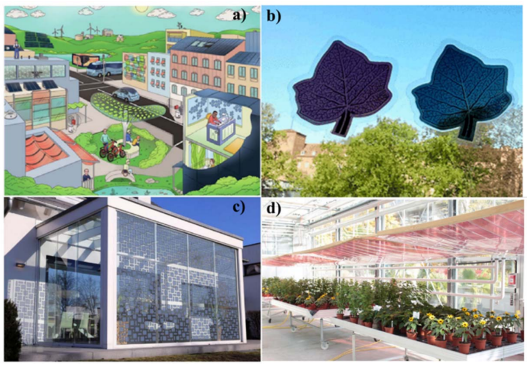

Figure 1. (a) Vision of 'energy anywhere at any time' by the integration of printed PV into automotive applications, bags, urban furniture, facades, awnings, windows, and indoor energy harvesting equipment. Reproduced with permission from the energy campus nürnberg. Reproduced from [2]. © The Author(s). Published by IOP Publishing Ltd. CC BY 4.0. (b) ivy leaf shaped organic solar modules, using different colors. [3] John Wiley & Sons. [© 2015 WILEY-VCH Verlag GmbH & Co. KGaA, Weinheim]. (c) Integration of OPV modules in glass windows. Reproduced from [2]. © The Author(s). Published by IOP Publishing Ltd. CC BY 4.0.

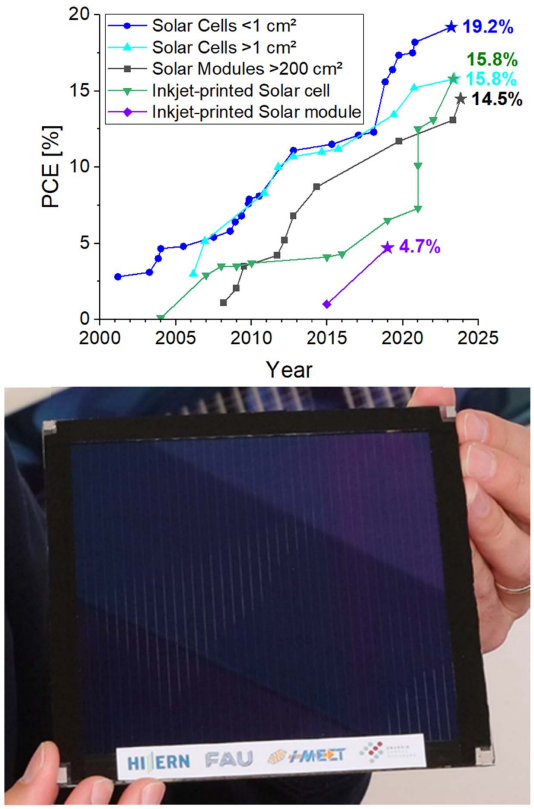

Figure 2. (a) Recent developments of high-performance OSC cells and modules according to NREL efficiency charts [5–7] and developments of solar cell and module efficiencies, where at least the active layer was inkjet-printed (see table 2) (b) current world record OPV module by FAU/FZJ. Reproduced with permission of HIERN/Kurt Fuchs.

level [8–18]. Upscaling efforts led to the fabrication of world record organic solar cell (OSC) modules reaching from 11.7% by Distler *et al* in 2019, to 13.1% by Waystech and recently 14.5% by Basu *et al* in 2023 as displayed in figure 2(b) [7, 19, 20].

Commercialization of OPV requires high throughput production at reasonable cost for investment and operation. Roll-to-roll (R2R) manufacturing of organic solar modules by printing on flexible substrates has great potential to meet this requirement [21, 22]. To achieve maximum throughput at minimum cost, the modules should be all-solution processed. However, all the devices with champion efficiencies use at least one layer that is not solution processed. Therefore, research on all-solution processed devices, from bottom to top electrode, is in the focus of current investigations, 15.3% PCE having been demonstrated by the groups of Jiang *et al* [23].

Successful upscaling of the OPV technology by all-solution based production processes requires a detailed and complete understanding of the specific challenges of this PV technology. As OSCs consist of 5 different layers it is necessary that orthogonal solvents are used for depositing consecutive layers, which however makes the deposition processes prone to dewetting [24]. Another challenge is controlling the formation of the proper bulk heterojunction morphology (BHJ)of the active layer during drying. It is mainly this metastable morphology that defines performance and lifetime of the devices. It can be adjusted by processing parameters like drying temperature, solvents, additives, and other variables [25–28]. One of the most critical aspects in the production of all-solution processed devices is the deposition of appropriate electrodes, consisting, e.g. of silver nanoparticles (AgNP) [29], silver nanowires (AgNWs) [30–33],conducting polymers [34, 35], and composites [36, 37]. Solution processed top electrodes can easily damage the layers underneath, due to solvent or material ingress. Furthermore, they usually do not from completely dense layers and consequently do not protect the device from ambient effects as well as evaporated electrodes do. For bottom electrodes, roughness is a critical point, as too high roughness leads to the penetration of the active layer, which is only a few hundred nanometres thick in OPV devices, and thus to a contact of the bottom with the top electrodes, called shunt [38, 39]. Finally, a certain number of solar cells must be connected monolithically to modules to realize devices with appropriate voltages and reasonable power output at low resistive losses, which introduces additional challenges [40]. The larger the area of the module the higher is the probability of defects like shunts or high interconnect resistances. Moreover, the total interconnect area, which does not contribute to the current of the module, should be as small as possible to provide high geometric fill factors (GFF). These additional challenges are the reasons why the module performance always lags behind the cell performance,

as it is obvious from figure 2. For inkjet-printed modules the cell-to-module gap is still huge.

Any commercially successful production technology must be able to cope with the challenges described above. We will explore in the following the potential of inkjet printing in this respect and how the traits of this printing technology can be employed beneficially for creating new opportunities for OPV, e.g. by enabling OPV modules with unique design features or by energizing discretionary 2D and 3D surfaces.

1.2. Modern production technologies of oPV devices

Table 1 gives an overview of the most popular manufacturing techniques of 'printed' PV. Comparing all these technologies, inkjet-printing is the only one that meets the essential requirements of production technologies for commercial OPV products. Free color and free form printing, easy layout changes together with R2R printing R2R capability, high throughput, low production costs and low material waste have already been demonstrated everywhere in industry for all kinds of inkjet-printed products like labels, posters, cards and so forth. Especially low material waste is of importance in OPV printing as functional organic materials are quite expensive. On top, inkjet-printed layers, can be deposited on any type of material due to their contact-less deposition, resulting in OPV with ultralight weight or on discretionary surfaces like directly on IoT devices, facade materials with low fire load and many others without additional patterning methods (figure 1). The implementation in already existing printing sites is relatively straightforward, which is one of the reasons why inkjet printing in the field of optoelectronics has developed very well in the past years. It has already been shown that organic light emitting diodes (OLED) [41, 42], organic field-effect transistors [43, 44] and fully inkjet-printed OSCs [45, 46] can be realized by this technology. This opens the market towards commercial printing of different organic optoelectronics with only one high throughput printing technology that is capable of realizing the visionary concept shown in figure 1(a). Consequently, inkjet-printing is the best choice for upscaling and mass production.

1.3. Recent advances in inkjet-printed OPV

Table 2 provides an overview of important steps towards all inkjet-printed OSCs and modules. For a detailed account of the development of inkjet-printed OPV, we refer the reader to several excellent reviews.

Maisch *et al* presented a brief overview of advances in inkjet-printed OPV before 2020 [45, 47], while Chen *et al* continued with more recent developments [48]. Bastola *et al* show pathways towards 3D printed electronics [49], while Xia *et al* demonstrate different printing technologies in OPV [50] and Lohse discuss fluid dynamic challenges in inkjet-printing [51]. Here we will thus focus on the most recent advances and remaining challenges on the path towards fully and all inkjet-printed OPV devices with a focus on upscaling and industrialization.

Inkjet-printing of OPV goes back to 2004 and has resulted in current record PCEs of 15.8% realized by Sang *et al* who prepared devices in which the PBDB-T-2F:BTPBO-4Cl:$PC_{61}BM$ active layer was ink jet printed [52]. Printing the whole layer stack is much more difficult, especially the printing of smooth electrode surfaces that do not generate shunts. Consequently, fully inkjet-printed solar cells (all layers printed on a pre-fabricated conductive substrate, such as glass/ITO) and all inkjet-printed solar cells (all layers, including the bottom electrode, printed on a non-conductive substrate) usually show lower performances compared to cells with e.g. sputtered ITO electrodes. The recent record in fully inkjet printing OPV on ITO substrates was achieved in 2021 by Baran *et al* with 9.58% PCE [53].

The latest achievements in all inkjet-printed OPV, from bottom electrode to top electrode, were made by Maisch *et al* with 4.3% and 4.7% PCE [30, 45] (on glass) and by Baran *et al* with 4.73% PCE (glass) and 3.61% PCE (parylene).

Finally, the very first fully and all inkjet-printed OSCs on 3D substrates were realized recently by Steinberger *et al* reaching 7% on 3D glass/ITO substrates and 2.5% PCE on 3D glass substrates, respectively [68]. These achievements have been described in detail in previous reviews [47, 48, 51, 69].

The main focus of the present review is on the specific challenges and solutions towards successful commercialization of inkjet-printed OPV modules. We will summarize several design rules that can help to bridge the gap between lab and fab of the OPV technology. We will conclude the review with examples of applications and production methods where inkjet-printed OPV may have an advantage over other technologies by making use of its unique traits.

2. Challenges and opportunities towards commercialization (Inkjet printing of PV devices and its specific challenges)

In this section, we will discuss the recent developments in inkjet OPV printing technology under the aspect of its successful commercialization. The commercial success of PV technologies has historically been determined in terms of the magic triangle of PV, consisting of efficiency, lifetime and cost. Inkjet-printed OPV adds further aspects, which represent superior design of PV panels, functionalization of discretionary surfaces with PV, as well as ultralight-weight solar modules, thus enabling a large variety of niche applications, which cannot be catered for by classical PV technologies.

Table 1. Comparison of coating and printing technologies [47, 48].

Technique	Ink viscosity	Resolution	Waste	Free- form	Multi-color	Pattern	Through-put	Challenges
Spin coating	⩽50 cP	—	Very high (up to 90%)	No	No	No	Low	Upscaling
Blade coating	⩽3000 cP	—	Low	No	No	No	Low	Upscaling
Spray coating [54–63]	⩽100 cp	Only with mask	Medium, high with mask	With mask	Maybe	With mask	High	Film homogeneity, shunts
Slot-die coating [64]	⩽10 000 cP	20 μm in combination with laser patterning	Low	No	No	1-D	Very high	Module fabrication requires combination with scribing by needles or laser
Gravure printing	⩽5000 cP	10 μm	Low	Limited	No	2-D	Very High	Viscosities of most inks too low
Aerosol-Jet printing [65–67]	⩽100 cp	20 μm	Low	Yes	Yes	3-D	Low	Shear forces during printing, coffee ring effect
Inkjet-printing	**⩽30 cP**	**20 μm**	Low	**Yes**	**Yes**	**3-D**	**High**	Multiple strict requirements with respect to ink properties, nozzle clogging, coffee ring effect

Table 2. Important developments of inkjet-printed OPV cells and modules from 2004 until 01/2024[63, 64].

References	Year	Inkjet-printed material	Comment	PCE (%)
[70]	2004	P3HT:C60a)	First inkjet-printed BHJ	< 0.1
[71]	2007	P3HT:PC60BM	First efficient inkjet-printed BHJ-using new solvent system oDCB:mesitylene	2.9
[72]	2008	P3HT:PC60BM	New record efficiency, oDCB:mesitylene solvent system with 96%RR P3HT, elevated temperature printing	3.5
[73]	2009	PEDOT:PSS	Use of glycerol as additive for conductivity improvement and EGBE surfactant for better wetting	3.2
[74]	2010	P3HT:PC60BM	New solvent systems with different mixtures of chlorobenzene and trichlorobenzene and 130 °C optimized drying temperature	2.4
[75]	2010	PEDOT:PSS P3HT:PC60BM	Use of the high boiling point additives ODT, ODCB and Cl-naphthalin improved solar cell performance due to better morphology, ODT gave best efficiency	3.7
[76]	2010	ITO nanoparticles	Thermal annealing at 450 °C resulting in 84% transmittance (T) and 207 Ω/sq sheet resistance (Rsq)	2.1
[77]	2011	PCPDTBT:bis-PC60BMd), PCPDTBT:PC60BM PSBTBTe):PC60BM	Combinatorial screening with morphology investigation	- 1.5 0.6
[78]	2012	Ag grid front electrode PEDOT:PSS	Effect of grid and busbar height measured and simulated	1.5
[79]	2013	Ag grid back electrode Ag full back electrode	Alternative to evaporated metal electrode	1.6 2.0
[80]	2013	PFDTBTP f):PC60BM	Chlorine-free solvent system based on anisole and THN	2.7
[81]	2014	PEDOT:PSS/ PCDTBT:PC70BM/ ZnO nanoparticles Ag full back electrode	First report of **fully** inkjet-printed OPV	2.0
[82]	2015	AgNW back electrode	Poor mesh uniformity resulting in 44.9 Ω/sq at 86% average transparency	2.7
[83]	2015	PEDOT:PSS P3HT:PC60BM ZnO nanoparticles	**Modules** on 92 cm^2 active area with non-halogenated solvents (evaporated electrodes)	1.0
[84]	2015	Ag grid front electrode ZnO nanoparticles PEDOT:PSS P3HT:PC60BM or PV2000g):PC60BM PEDOT:PSS Ag grid back electrode	**Fully** inkjet-printed devices, Freedom of form demonstrated: solar cell with shape of Christmas tree	1.7 4.1
[85]	2016	P3HT:ICBAh) Nanoparticles	Printing of eco-friendly active layer nanoparticle dispersion	2.9
[30]	2016	AgNW ZnO PV2000:PC70BM PEDOT:PSS AgNW	**Fully** inkjet-printed devices, Semitransparent, 1 cm^2	4.3
[86]	2018	PEDOT:PSS	Combination of solvents and surfactants to improve wetting on active layer	1.9
[87]	2018	Nano-graphite	inkjet-printed nano-graphite as PEDOT:PSS replacement	2.4
[88]	2019	P3HT:O-IDTBR	Printed non-fullerene acceptors Halogen free solvents Free shape OPV cell in the shape of a turtle	6.5 4.5 4.8
[45]	2019	AgNW:ZnO PV2000:PC70BM AgNW:PEDOT:PSS	**All inkjet-printed solar modules** on 10 cm^2 active area, Free shape R2R inkjet-printed solar modules	**4.7** **4.3**

(Continued.)

Table 2. (Continued.)

References	Year	Inkjet-printed material	Comment	PCE (%)
[46]	2020	ZnO P3HT:O-IDTBR PEDOT:PSS Ag	Light weight fully printed solar cells on parylene **Fully printed solar cells**	**3.6**
[89]	2021	p-DTS(FBTTh$_2$)$_2$:PC$_{70}$BM	Systematic study of the Influence of Inkjet-printing parameters on morphology; Donor crystal sizes decreased with printing speed and substrate temperature increasement; π-π stacking distance decreased with increasing inkjet printing speed	7.3
[53]	2021	PEDOT:PSS Ink engineering of transport layers **Fully printed solar cells on ITO**	Non-fullerene solar cells PTB7-Th:IEICO-4F AZO nanoparticle Ag nanoparticle	**9.6**
[90]	2021	PM6:ITIC-4F	Non-fullerene solar cells with non-halogenated solvents	10.1
[53]	2021	PTB7-Th:IEICO-4F	Non-fullerene solar cells	12.5
[91]	2022	PBDB-T:ITIC	Non-fullerene solar cells one step printing	6.4
[91]	2022	PBDB-T-2F:BTP-BO-4Cl	Non-fullerene solar cells, layer-by-layer printing	13.1
[92]	2023	Graphene ink	HTL development: inkjet-printed graphene in P3HT:PC60BM OPV	2.0
[52]	2023	PBDB-T-2F:BTP-BO-4Cl	Ink solvent and temperature optimization in NFA solar cells	14.0
[52]	**2023**	PBDB-T-2F:BTPBO-4Cl:PC$_{61}$BM	Ink solvent and temperature optimization in NFA solar cells; DCB and TMB solvents were mixed with THN for improved morphologies and reduced drying lines at high temperature drying	**15.8**
[68]	2024	ZnO PV2000:PC60BM PEDOT:PSS AgNW	**Fully inkjet-printed solar cells on ITO 3D surface**	7.0
[68]	2024	AgNP ZnO PV2000:PC60BM PEDOT:PSS AgNW	**All inkjet-printed solar cells on 3D surface**	2.5

As shown previously, inkjet printing has several advantages towards industrially relevant PV production, but several points still need to be tackled to fully commercialize the technology. Main aspects that have to be considered on that route are the effects of inkjet-printing on solar cell efficiency and lifetime, cost reduction with efficient upscaling and pathways to conquering niche markets.

The main challenge, that needs to be solved for successful commercialization of inkjet printing lies in the multitude of requirements an industrial ink has to fulfill simultaneously (figure 3). Besides stable drop formation, one of the biggest issues is nozzle clogging, meaning that due to solvent evaporation or aggregation of the solid content of the ink, the inkjet nozzles are clogged so that drop ejection is not possible anymore. Further challenges are the wetting on the substrate, drying behavior with possible coffee ring effect and the film formation with a proper nano-morphology and surface topology. These requirements are often conflicting, as will be detailed below. This makes ink engineering a central part of the development towards industrial printing of OPV.

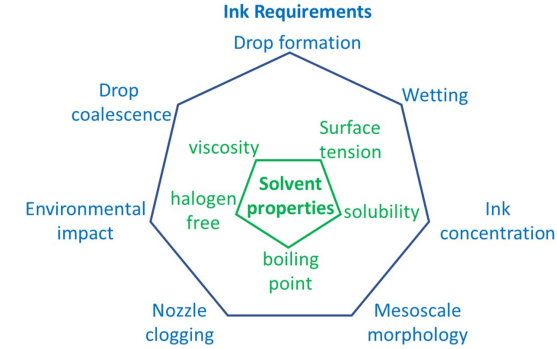

Figure 3. Overview of Ink requirements and the corresponding solvent (mixture) properties,

2.1. Stable drop formation and nozzle clogging

First of all, stable drops have to be formed at the nozzle. In piezo drop-on-demand (DOD) inkjet

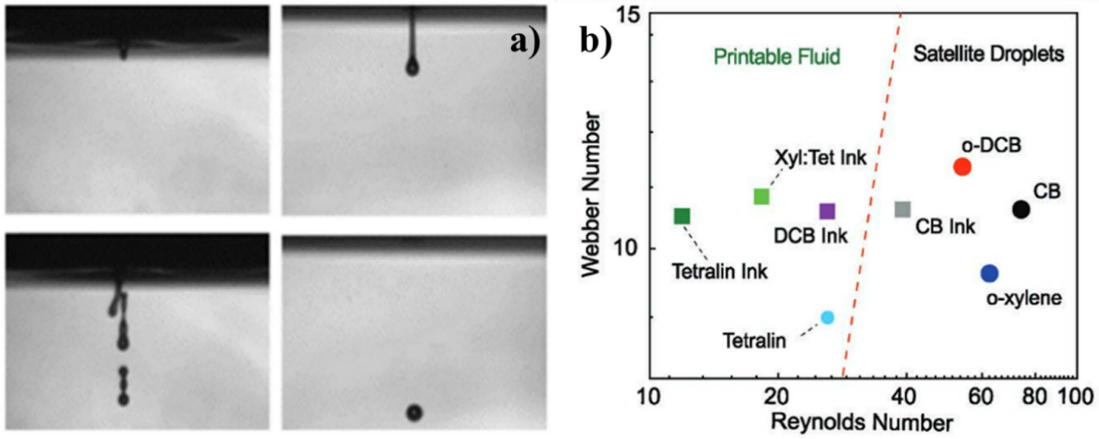

Figure 4. (a) Different drop formation depending on the piezo pulse and ink properties. Reprinted from [96], Copyright (2005), with permission from Elsevier; (b) Proper ink design by Baran *et al* for printable active layer inkjet inks. [88] John Wiley & Sons. [© 2019 WILEY-VCH Verlag GmbH & Co. KGaA, Weinheim].

printing, a short voltage pulse within the piezoelectric element creates the force for drop ejection [93, 94]. Each pulse has to create an individual spherical droplet as any issue here may lead to device failure of a printed electronic device [95]. For this reason, the fluid properties are crucial in order to create a stable inkjet printing process (see figure 3). As described elsewhere [47], the three dimensionless numbers Ohnesorge (Oh), Reynolds (Re) and Weber (We) define the stable printing region and are mainly dependent on viscous and surface forces (see equations (1)–(3)).

$$\mathrm{Re} = \frac{\text{inertian forces}}{\text{viscous forces}} = \frac{\rho \times u \times l}{\mu} = \frac{u \times l}{\nu} \tag{1}$$

$$\mathrm{We} = \frac{\text{inertian forces}}{\text{surface forces}} = \frac{\rho \times u^2 \times l}{\gamma_L} \tag{2}$$

$$\mathrm{Oh} = \frac{\text{viscous forces}}{\sqrt{\text{inertial forces} \times \text{surface forces}}}$$

$$\mathrm{Oh} = \frac{\sqrt{\mathrm{We}}}{\mathrm{Re}} = \frac{\mu}{\sqrt{\rho \times \gamma_L \times l}} \tag{3}$$

where ρ is the liquid density, u the speed, γ_L the surface tension of the ink, μ the dynamic viscosity, ν the kinematic viscosity and l is a characteristic length scale (for inkjet typically the nozzle or drop diameter).

Inadequate ink properties lead to either satellite droplets, splashing, ink dripping or even no drop formation at all, as shown in figure 4 for different Re numbers [96]. Typical Re numbers need to be between 10–100 for ejection of droplets and between 10–40 to avoid satellite droplets, typical We numbers between 5–15 and Oh numbers should be in the range between 0.1–1. As a consequence, for every ink the viscosity needs to be tuned carefully, together with the piezo pulse, to create stable droplets [45].

Common inks for inkjet-printing of the active layer of OPV devices comprise solvents like chlorobenzene (CB), o-DCB and, as main non-halogenated solvent, o-xylene (OX). Unfortunately, these solvents are not suitable for stable inkjet printing. Due to their low viscosities, resulting in high Reynolds numbers, they are in the regime of satellite droplets and have to be modified accordingly (figure 4). The workaround for this problem is the use of high-boiling additives of higher viscosities, which decrease the Reynolds number and simultaneously prevent nozzle clogging by slower solvent evaporation. Suitable Re numbers for inkjet-printing are between 10–30, what was realized by Baran *et al* and Maisch *et al* who developed several inks based on tetralin that lead to better printability of the resulting active layer ink [45, 88]. Another approach of Maisch *et al* and Baran *et al* is based on the increase of the polymer concentration that leads to proper viscosity ranges for printing (figure 4(b)). Table 3 summarizes the possible measures for the formulation of active layer inks which meet the requirement of stable drop formation.

2.2. Enhancing the efficiency of inkjet-printed OSCs

Due to the recent advances described above (see table 2) [45, 52, 53, 88, 91, 97], inkjet-printed OSCs have reached PCE's of around 16%, which are similar to PCE values achieved by other liquid phase-based production techniques and will further increase as active layer systems will be improved. As such, the efficiencies of inkjet-printed OPV are expected to get closer to the efficiencies of inorganic PV technologies.

The efficiency of OPV is directly dependent on the nano-morphology of its respective layers. The understanding and control of the drying process, that leads to the desired morphology is more challenging for inkjet-printed films as compared to other industrially relevant coating techniques, for two main reasons. First, as discussed above, the constraints

Table 3. Active layer ink formulation and its consequences towards printability and efficiency.

Ink property	Consequences for printability	Consequences for performance
Amount of low boiling point solvent	High Reynolds numbers of common solvents lead to satellite droplets Low boiling point lead to faster evaporation and thus nozzle clogging	Enhances drying speed, leading to better performance
High boiling point additive	Lower Reynolds numbers lead to better printability High boiling point lead to slower evaporation, thus less nozzle clogging	Enhances drying time, leading to larger extent of phase separation and lower Performance
Polymer concentration	Different concentrations change Oh, Re, We and can thus adjust the printing regime, but higher concentrations lead to more probability for aggregation and nozzle clogging	Depending on the temperature and solvent leading to pre-aggregation and worse performance
Additives (e.g. solvents, small molecules …)	May change printability positively or negatively depending of the amount of additive	May increase or decrease performance depending on the amount of additive

regarding the printability of the ink set different or higher requirements for the choice of the ink (solvent, concentration) and the process temperature. This results in the development of specific inks and the choice of specific coating conditions. The behavior of the inkjet-printed wet films upon drying might therefore be completely different as compared to other printing techniques, and this might impact the dry layer quality. Second, the drying behavior of droplets is different as compared to layers. Additional physical processes like inhomogeneous evaporation, capillary flows or contact line pinning might alter the final deposition pattern and the conditions during morphology formation of the active layer. Consequently, challenges regarding the film formation and influencing the efficiency, like well-defined nano-morphology formation, good wetting, reduction of coffee rings and homogenous interlayer printing, need to be tackled.

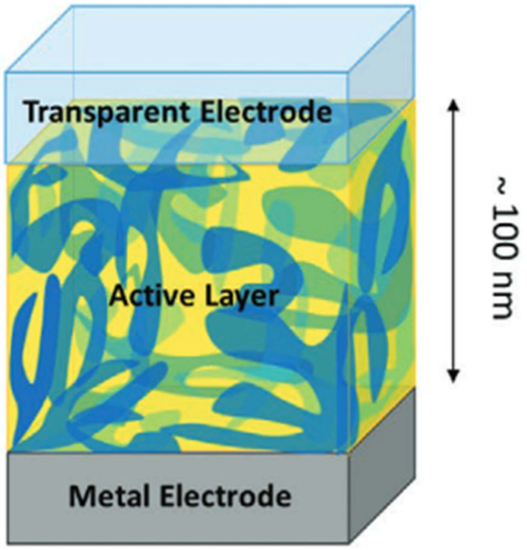

Figure 5. Schematic of a bulk heterojunction organic solar cell. [98] John Wiley & Sons. [© 2020 Wiley-VCH GmbH].

2.2.1. Theoretical considerations of bulk-heterojunction formation during drying

One specificity of OPV is the strong influence of the photoactive layer morphology on the device performance. OPV active layers are mostly based on blends of at least one donor and one acceptor material, which form a so-called 'BHJ' at the nanometer scale (see figure 5).

This BHJ consists of intermixed and pure domains of both materials to ensure proper charge generation and extraction. crystalline regions are also desired for optimal transport properties [98]. Such BHJ morphologies result from liquid-liquid phase separation and crystallization processes that mainly take place during the drying of the wet film, and which almost stop once the dry, solid state is reached [25]. All these phenomena depend on the choice of the solvent mixture and processing conditions, which impact physical parameters such as the solvent evaporation rate, the ink viscosity, the solubility and miscibility of the photoactive materials, as well as the precipitation properties. As a result, the constraints imposed by the need for inkjet printable materials might result in sub-optimal active layer morphologies. Modelling the process of BHJ formation can help to gain control over this morphology and to reach the properties that can already be obtained with other printing techniques. An appropriate model for such a non-equilibrium thermodynamic process should account at least for evaporation, liquid-liquid demixing, as well as crystal nucleation and growth-all in a wet film featuring highly concentration-dependent kinetic properties [25, 99, 100]. Different approaches have been proposed to gain insight into the photoactive layer formation of OSC. On the one side, most of the community's theoretical understanding is based on rather decoupled, qualitative arguments using for instance the Flory–Huggins theory

of blend miscibility [101–103], the evaluation of the donor-acceptor phase-diagram assessing crystallization thermodynamics [104–107], the solvent vapor pressure or boiling points, and the evaluation of diffusion properties [108–110]. On the other hand, due to the length (from a few nanometers to micrometers) and time (up to minutes) scales involved and the outmost importance of the kinetic quenching, small scale simulations like molecular dynamics and dissipative particle dynamics can only provide limited insights [111, 112].

At the end, thermodynamic continuum mechanics simulations turn out to be the most appropriate to tackle this problem. In this context, mostly phase-field simulations have been used in the field of OPV. As a first step, the spinodal decomposition of a dry donor-acceptor blend and its impact on device performance has been investigated by Alam and co-workers in the early 2010s [113, 114], followed by more recent work [115–118]. In their pioneering works, Michels and co-workers [119, 120] and Wodo and co-workers [121–123] first simulated the liquid-liquid demixing of OPV donor-acceptor blends during film evaporation. They highlighted the role of the evaporation rate, material miscibility and substrate properties. Furthermore, crystallization in a drying film has been considered recently by Michels, in the context of meniscus guided coating [124].

However, the first theoretical framework taking into account all the physical processes that are relevant for printed PV together has been developed only recently by Ronsin and co-workers [100, 125]. High-precision simulations of the formation of crystalline OPV BHJ matching the experimental observations have been demonstrated [126]. Crucially, as illustrated in figure 6, it allows to investigate how the BHJ morphology does not only depend on the donor and acceptor material properties, but also on the processing conditions. These include the choice of the solvent, temperature, or the evaporation rate. Typically, increasing the evaporation rate limits the time for morphology development, which might be either detrimental (if the phase separation hardly develops as desired), or positive (if the phase separation develops too far). Playing with the processing temperature, the type of solvent or additives is subtler from the theoretical perspective, because these parameters not only impact the evaporation rate, but also the kinetics of demixing, crystal nucleation and growth. Overall, getting an overview of process design rules using these theories is the topic of current research. Thereby, it must be highlighted that the design rules fully depend on the physical properties (solubility, miscibility, aggregation and crystallization tendency) of the considered optoelectronic materials. Even if this approach has not been applied to inkjet printing yet, it seems appropriate to answer two basic questions without significant additional developments: first, how do the solvents and processing conditions choices related to printability impact the active layer formation? Second, how does the BHJ formation in drying droplets compare to the one in a drying film?

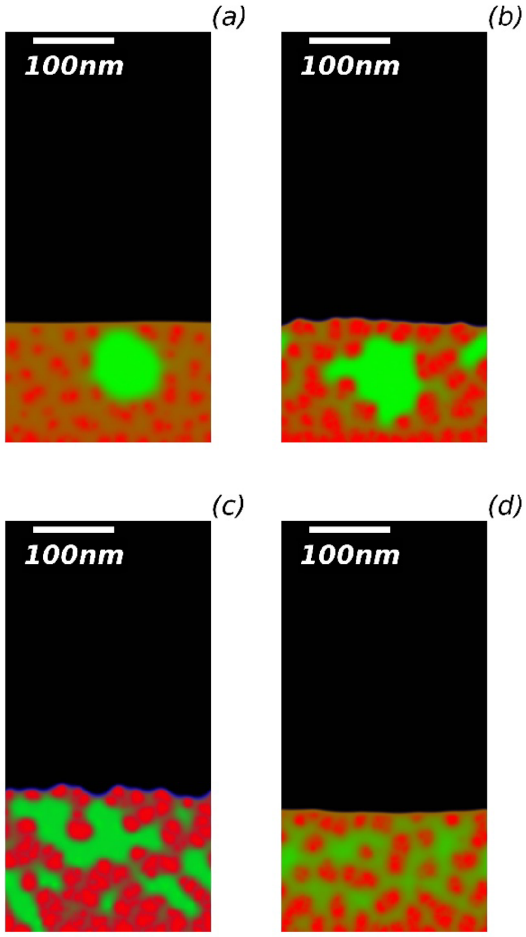

Figure 6. BHJ morphology at the end of the drying of a P3HT-DCB blend cast from DCB. The snapshot shows 2D cuts of the volume fraction fields, whereby green stands for PC60BM and red for P3HT. Deep red regions are P3HT crystals. (a), (b), (c) processing effect: increasing evaporation rate from left to right. (d) Material property effect: increased donor-acceptor compatibility. Reprinted with permission from [126]. Copyright (2022) American Chemical Society.

2.2.2. Efficient nano-morphology formation in inkjet-printed bulk-heterojunction OSC's

Common highly efficient OSCs comprising non-fullerene acceptors (NFA) use low boiling solvents like chloroform and CB. As previously described for inkjet-printing inks some high boiling additive is necessary to create a non-clogging and stable inkjet-printing process. Unfortunately, most current photoactive materials have poor solubility in high boiling point solvents, such as ortho-dichlorobenzene (oDCB), resulting in a large phase

separation of the BHJ film morphology and consequently compromised device performance. Here the ink requirements related to nozzle clogging, drop stability and morphology formation, as illustrated in figure 3, result in a competition between solar cell efficiency and printing stability.

The main processing strategies to improve BHJ morphologies in inkjet-printed OSCs are the same as for other printing and coating methods and are already very well reported in the literature [25–28]: (i) the reformulation of the inks with suitable solvent mixtures that still enable homogenous layers together with good morphologies [127, 128], (ii) the change of the drying process, e.g. by adjusting the temperature [64, 129], and (iii) the use of low amounts of liquid or solid additives that promote good crystallization [130–132]. These strategies will be described in detail in the following.

2.2.2.1. Solvent mixtures of efficient OSCs

For inkjet-printed OPV several approaches have been reported to control the nano-morphology of the active layer, while still assuring a stable printing process. Proper solvent mixture design is the major solution for stable inkjet printing, while still achieving good morphologies. Maisch *et al* developed tetralin (THN) as additive to OX for efficient inkjet-printed active layers (P3HT:PC60BM, PV2000:PC60BM) resulting in proper nano-morphology, less nozzle clogging and good printability [45]. Other researchers used the same solvent mixture for more efficient systems like PTB7-Th-IEICO-4F [53] and PM6:ITIC-4F [90], reaching 9.8% PCE and 10.1% PCE respectively and demonstrating the general approach for this solvent additive. Corzo *et al* further improved the solvent mixture approach and showed the influence of different active layer ink solvents on the morphology of the active layer. Their PTB7-Th-IEICO-4F system printed from CB: chloronaphthalene (CN) mixture resulted in 12.5% PCE compared to 9.8% PCE for OX:THN and only 8.2% with CB as solvent, reaching the same efficiency as a spin coated device with 12.6% PCE. On top, they demonstrated that the solvent mixture changed the vertical phase separation leading to different wetting behavior on the top of the active layer. Here the CB:CN solvent mixture leads to a more PTB7-Th rich surface, which resulted in the improved efficiency (see figure 7) [53]. What was not investigated in this respect yet is, that due to different solubilities of active layer materials in e.g. tetralin so-called preaggregation may happen before drop impact, meaning that small molecules may have formed small aggregates in solution before the drying process started. In addition, drying of the droplet during flying may lead to higher concentration of the active material in the droplet, resulting in preaggregation as already observed for OPV systems using PM6:Y6 in OX [64, 128]. This can especially be the case for printing onto 3D objects where the distance

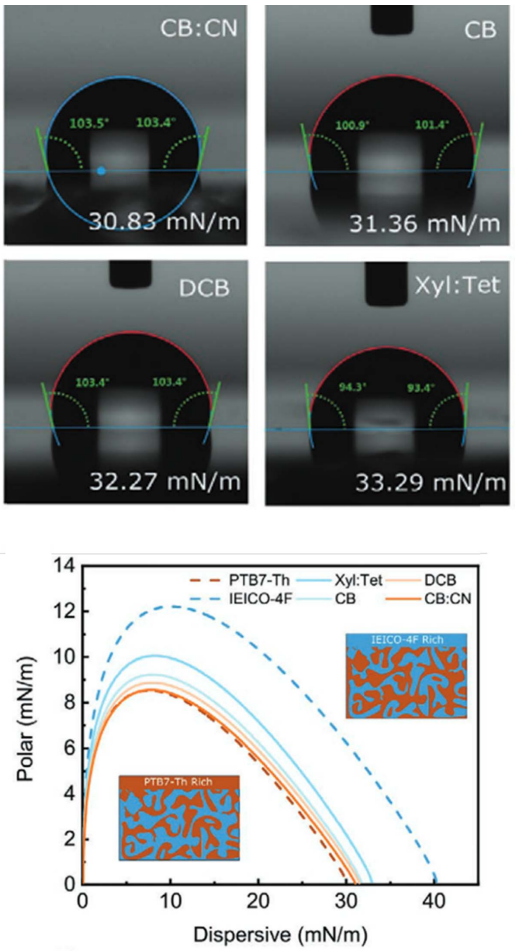

Figure 7. Top: Water contact angle on PTB7-Th:IEICO-4F layers printed from CB:CN, CB, DCB and O-xylene:tetralin solvents, bottom: calculated wetting envelopes of PTB7-Th, IEICO-4F layers compared with wetting envelopes of PTB7-Th:IEICO-4F layers printed from CB:CN, CB, DCB and O-xylene:tetralin solvents. [53] John Wiley & Sons. [© 2020 Wiley-VCH GmbH].

between the object and the nozzle is increased for better printing process stability. Multi-nozzle printheads may hit 3D objects for very small distances, especially in the case of slightly concave surfaces. In these cases, one would need to use only few nozzles on the side of the printhead to not interfere with the object. Consequently, for multi-nozzle inkjet printheads the distance to the object may be higher in order not to hit the 3D object with any part of the printhead. This leads to a variation of the number of usable nozzles, thus speeding up or slowing down the overall process. Changing the drying behavior is then another natural consequence for proper morphology formation control.

2.2.2.2. Drying time variations for efficient OSCs

As previously explained, one main point for nano-morphology formation is the drying time that can be controlled by the temperature. Additionally, temperature can trigger other effects like the coffee ring effect, nozzle clogging due to evaporation of

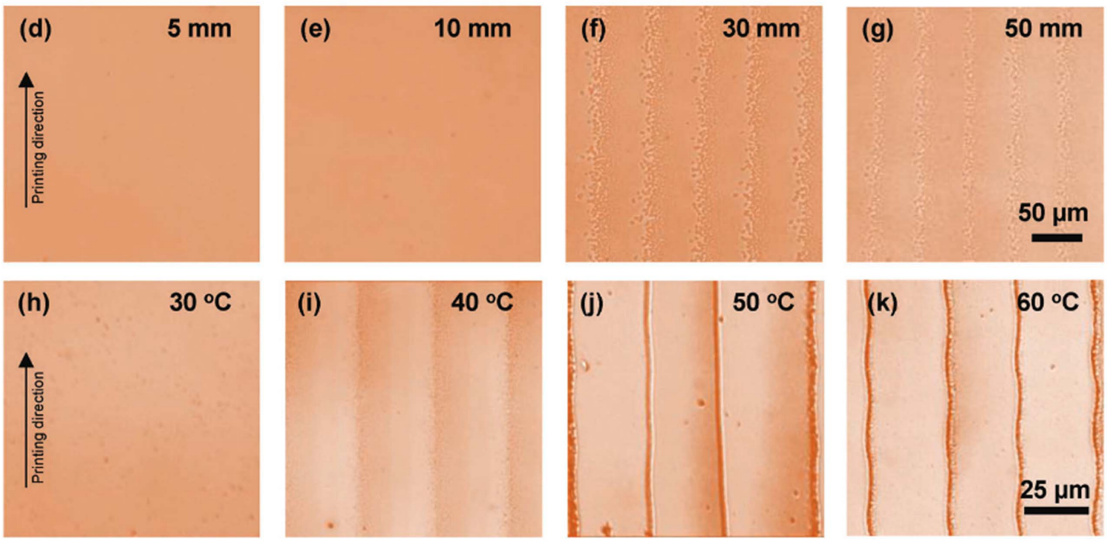

Figure 8. (d)–(g) Optical microscope photograph of PBDB-T-2F:BTP-BO-4Cl blend films with different film sizes. (h)–(k) Optical microscope photograph of PBDB-T-2F:BTP-BO-4Cl blend films at different temperatures. [52] John Wiley & Sons. [© 2023 Wiley-VCH GmbH].

solvent at the nozzle or preaggregation in solution as explained in other chapters and demonstrated by the ink requirements (figure 3).

A good example for nano-morphology formation during inkjet-printing of large area devices was recently investigated by Sang *et al* [52] They checked the influence of printing large areas and small areas using different temperatures. Here they showed that the larger the printing area is, the more solvent has evaporated before the next printed path merges with the old one, resulting in specific printing lines. These are much more pronounced for higher temperatures and lead to different donor:acceptor ratios towards the resulting film (figure 8).

Here we see two effects, a pronounced vertical phase segregation due to miscibility differences in the main solvents, namely oDCB and trimethylbenzene (TMB), and fast drying of droplets or in this case droplet lines [52]. As evaporation at the rim of a droplet or at the rim of a line is faster than in the center, phase segregation is faster at this point, describing well the visible lines. For low temperatures, the drying is slower leading to no lines as droplets can successfully merge to one wet film and dry all together. Unfortunately, very slow drying of the active layer results in unfavorable morphologies that decreases the resulting PCE. As a consequence, increased drying temperatures are necessary to obtain efficient OSCs. To overcome the printing line issue and still achieve good performance they introduced THN as additional solvent and realized record efficiencies with 13.98% and 15.78% for binary and ternary OSCs, respectively [52].

Another example is given by Chen *et al* [91], who show the influence of temperature on vertical phase separation. Their results demonstrate that an increase in substrate temperature suppresses strong molecule aggregation of the active layer components due to the high drying speed, enhancing exciton dissociation efficiency and thus the short circuit current. Unfortunately, this has a negative effect on the vertical phase separation of donor and acceptor due to too fast drying directly at the hot substrate surface, giving donor and acceptor no time for vertical phase separation [91].

2.2.2.3. Drying time variations for efficient OSCs with different inkjet related parameter

Temperature variations were demonstrated for many different OPV production technologies. Nevertheless, there are several parameters exclusively related to inkjet-printing that can change the drying process as well. Drop spacing for example can change the layer homogeneity and thus performance drastically. The resulting line and consequently layer may be uniform for proper drop spacing and printing frequency or can be bulging, scalloped, isolated or stacked points depending on the spacing and time delay between two consecutive droplets (for more details see 2.3.1). Chen *et al* demonstrated this as well for PBDB-T:ITIC films and received an optimal drop spacing of 40 μm [91].

Not only does the drying temperature affect the drying speed but also the printing speed does. According to Lan *et al* low printing speed results in longer drying times due to thicker wet films and enhances phase segregation and domain size (see figure 9) [89]. They investigated as well the additional effect of printing temperature and came to the conclusion that higher temperature leads to the formation of even more nucleation sites, decreasing the crystal size-which is beneficial for

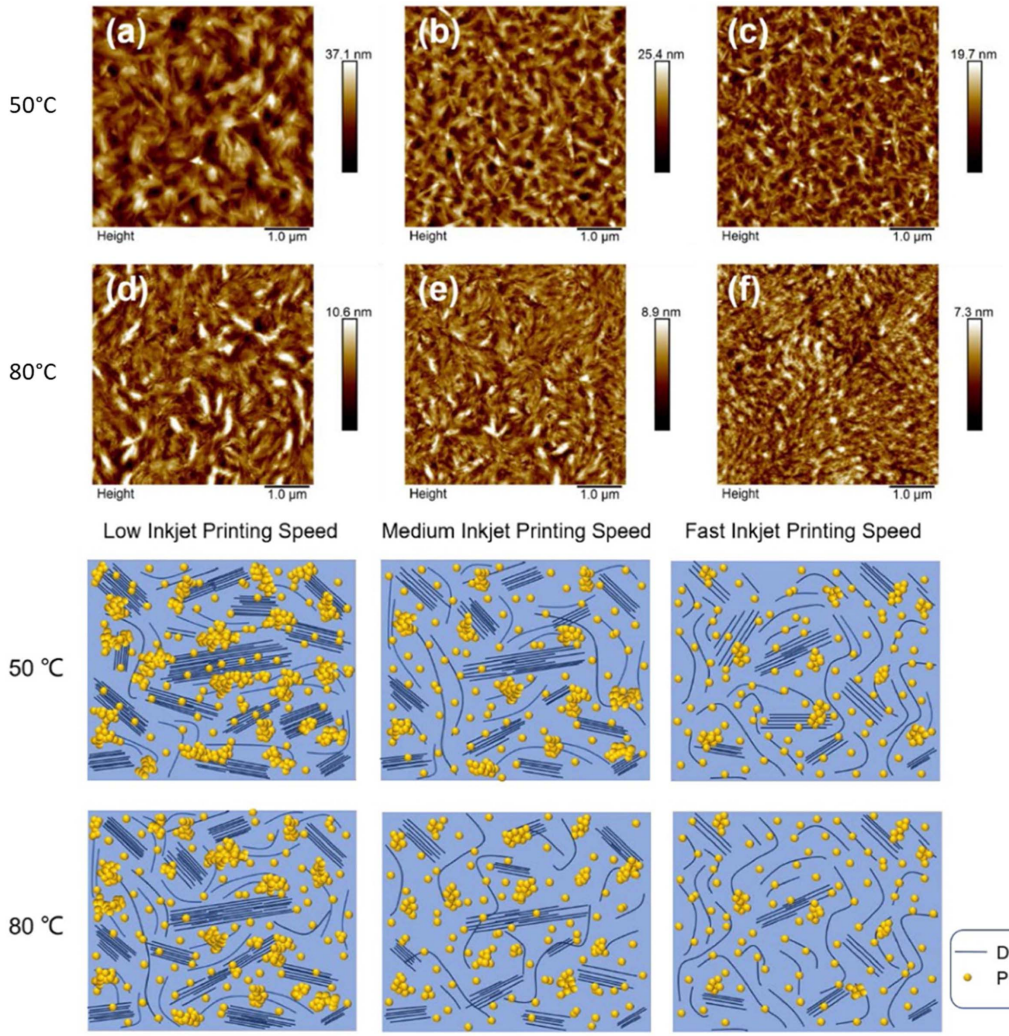

Figure 9. Top: AFM surface morphology of active layers from inkjet printing with different printing speed and drying temperature; bottom: schematic of the nanomorphology of the active layer from different inkjet printing speeds and substrate temperatures. Reproduced from [89]. © IOP Publishing Ltd. All rights reserved.

the performance-but at the same time results in an uneven film due to very fast drying, negatively affecting the performance.

2.2.2.4. Additives for efficient inkjet-printed OSCs

Only few inkjet-printed active layers use low amounts of liquid or solid additives, as they may result in nozzle clogging and affect the printing behavior. Lan *et al* used DIO as solvent-additive for CB to reach 7.3% PCE [89], while Sang *et al* achieved their record PCE with a ternary blend using $PC_{70}BM$ as small molecule-additive [52]. While most researchers focus more on solvent mixtures, where they use more than 10vol% of each solvent, the additive route is one of the least developed ones. Especially solid additives can be promising for further optimization of inkjet-printed active layers, but need to be handled with special care as particles may form additional agglomerates causing nozzle clogging or sedimentation as further discussed in 2.4.3.

Conclusively, the challenges for efficient inkjet-printed solar cells with respect to nano-morphology of the active layer are similar to the ongoing works in the field. Ink requirements for inkjet-printing influencing nozzle clogging, print stability or ink concentration (figure 3) add additional constraints, but also additional complexity to the system leading to more process optimization opportunities concerning the use of solvent mixtures and additives. Here simulations (see chapter 2.1.1) are of special relevance as they can help to reduce time and costly trial-and-error approaches for the optimization of solvent mixtures and additives [100, 126]. Proper choose of printing process parameters can also overcome the above-mentioned constraints [48]. The difference in evaporation time for high-boiling solvents in inkjet printing inks and low boiling solvents currently used in high-efficient OPV systems can for example be tackled by printing onto heated substrates. The faster drying process of droplets compared to wet films can even lead to too fast evaporation that

again results in the need for solvent adjustments for proper layer formation. Consequently, the use of process-structure-performance relationships in OPV as demonstrated above is necessary for commercialization. The main correlations learned so far are that wet film thickness and homogeneity increases with decreased drop spacing, faster printing speeds result in thinner wet films and higher temperatures lead to less phase separation due to faster drying. This can help to adjust the drying speed, which is relevant for optimal phase separation and aggregation. Too fast drying lead to well intermixed systems without proper phase segregation, while too slow drying lead to high phase separation, being both cases non-optimal for solar cell performance due to non-optimal charge extraction and transport. Additionally, solvent additives and mixtures can influence drying behavior and phase separation as well in all directions [48]. To further optimize the phase separation the concept of bilayer OSCs was applied as well to inkjet-printed OPV. Here DOD technology benefits its high precision as well as its non-contact processing.

2.2.3. Efficient nano-morphology formation in inkjet-printed bilayer OSCs

The record for inkjet-printed active layers from 2022 was realized by utilizing layer-by-layer (LbL) inkjet-printing. Chen *et al* created a layer by layer printed active layer, reaching 13.09% PCE for a PBDB-T-2F:BTP-BO-4Cl printed with o-DCB as solvent. Here they demonstrated that by printing the donor on top of the acceptor a BHJ with donor enriched surface and acceptor enrichment on the bottom side of the layer was produced (figure 10) [91]. This improved nanoscale phase separation led to higher J_{sc} as well as higher FF and V_{oc}, resulting in a record efficiency of 13.09% compared to only 13.56% for spin coated OSCs. For PBDB-T:ITIC the LbL method showed an improvement in Voc but overall worse performance due to re-dissolved ITIC resulting in poorer film quality. Consequently, the solvent design is crucial here as well. Overall, the LbL method is a promising way to improve bulk heterojunction vertical phase separation in order to achieve high efficiencies.

2.2.4. Wetting-the printing of electrodes and interlayers

The merging of droplets to form a dense film is an essential requirement for homogenous films and thus working devices. The distance between two droplets and the drop radius on the surface determines whether a continuous wet film is formed or not. The radius of the droplet on the surface is defined by the wetting angle and is thus the most important aspect for good layer homogeneity. A contact angle (CA) of 0° defines perfect wetting, whereas an angle less than 90 °C is still defined as good wetting. This is required for proper layer formation [45]. The concept of a wetting envelope helps to define how inks and solvents wet on a given substrate and how to change

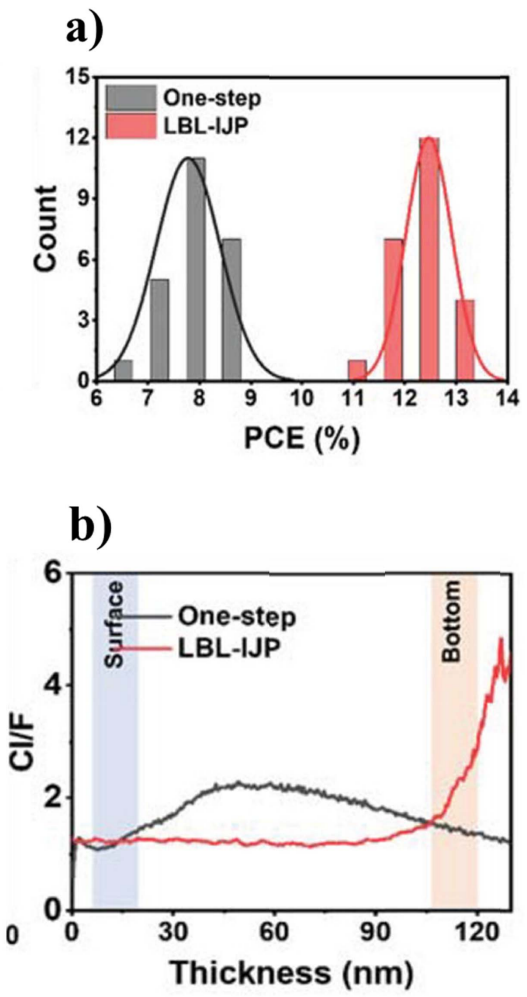

Figure 10. (a) Histogram of the one-step and LBL-IJP processed PBDB-T-2F:BTP-BO-4Cl OSCs and b) ToF-SIMS element profiles of PBDB-T-2F:BTP-BO-4Cl films from one-step and LbL-IJP. [91] John Wiley & Sons. [© 2022 Wiley-VCH GmbH].

polarity in order to reach suitable wetting angles [45]. A wetting envelope (solid line in figure 11) defines a constant CA (here 0°) for a given solvent with a certain dispersive and polar (LP) surface energy part. Solutions that lie within the envelope have a CA lower than the envelope angle (here 0° = perfect wetting). Changing the inks total surface energy or adjusting the dispersive and polar ratio of the surface energy is therefore needed to enable a certain CA. This is realized by tuning the ink solvents and the respective surface tension of the ink and demonstrates another part of the above-mentioned ink requirements (see figure 3).

Figure 11 shows examples of bad wettability of PEDOT:PSS on active layer films, where the inks are not within the respective wetting envelopes, due to too high surface energies (see water and PVP AL4083) and a mismatch in polar to dispersive parts of the surface energies. The main route to overcome this issue is the use of proper solvents or solvent mixtures that lie within the wetting envelope or additives.

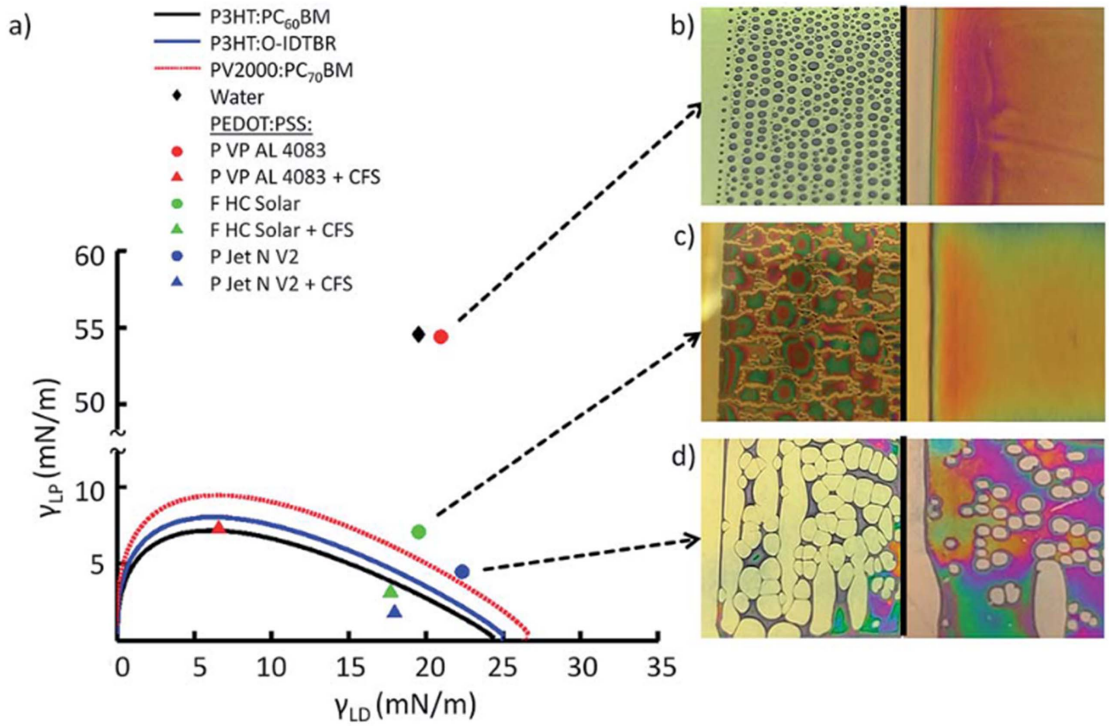

Figure 11. (a) Wetting envelopes of commonly used OPV active layer materials P3HT:PC60BM, P3HT:O-IDTBR and PV2000:PC70BM and surface tension data of PEDOT:PSS inks P VP Al 4083, F HC solar, P JET N V2. An amount of 0.1% wt wetting agent CFS was added to the PEDOT:PSS inks to lower the surface tension and improve wetting. Inks within the wetting envelope are expected to show complete wetting on the corresponding surface. Inks located outside are expected to show only partial wetting or dewetting. (b) Photographs (size: 1 cm × 1 cm) of dry inkjet-printed PEDOT:PSS layers from (left) P VP AL 4083 and (right) P VP AL 4083 + 0.1 wt% CFS, (c) (left) F HC solar and (right) F HC solar + 0.1 wt% CFS, (d) (left) P JET N V2 and (right) P JET N V2 + 0.1 wt% CFS on a P3HT:PC60BM surface. Reproduced from [137] with permission from the Royal Society of Chemistry.

The successful use of wetting agents in inkjet-printed PEDOT:PSS on an active layer is demonstrated by Maisch *et al* who used a fluorosurfactant from capstone (CFS), while Eom *et al* used EGBE [45, 73].

An overview of surface energies of different solvents, ETLs and HTLs was demonstrated by Baran *et al.* The comparison of these surface forces to the wetting envelope of PTB7-Th:IEICO-4F displays that common inkjet-printed ETL inks like AZO, ZnO [45, 133] and sol-gel [134] ETLs already meet the wetting requirements, while AI 4083 ink as common HTL material does not. In this work they invented a modified Ω-PEDOT ink that lies within the wetting region of PTB7-Th:IEICO-4F and showed that the use of alcohols like 1-butanol, IPA or 1-pentanol allows to tune the wettability (see figure 12(a)) [53].

Unfortunately, the modern PEDOT:F system, that is suitable for highly efficient NFA systems [23], has not been inkjet-printed yet, but using the aforementioned solvents one may be able to reformulate the IPA based PEDOT-F to a high boiling solvent like 1-pentanol. Other researchers focused more on solution processable metal oxides as HTLs and realized inkjet-printed NiO [135] and recent developments resulted even in a completely new approach, a green production of graphene ink for inkjet printing [92].

This new water-based inkjet-printing HTL layer, developed by Kastner *et al* can improve hole extraction and prevent charge recombination. As water does not wet onto active layers argon plasma was used to enhance wetting of this new HTL [92]. This and other surface treatments like ozone, interlayer coatings or smoothing layers are common ways to overcome wetting problems without changing the ink solvents (see figure 12(b)) [136].

If ink reformulation, additives or surface treatments are not possible due to constraints related to ink requirements or layer functionality, another good alternative is the use of pinning centers, as demonstrated by Maisch *et al* [137] Small droplets of dried ink act as anchoring sites for a homogenous thicker wet film leading to a homogenous wetting without the need of further ink changes or surface treatments [136]. This method can also be used for patterning of surfaces (see figure 13).

2.2.5. Coffee ring effect

Besides controlling the morphology of active layers, ensuring the proper formation and deposition of functional materials, including nanoparticles and polymers used in other layers, is crucial for achieving optimal device performance. As previously explained, droplet drying is one of the differences related to the

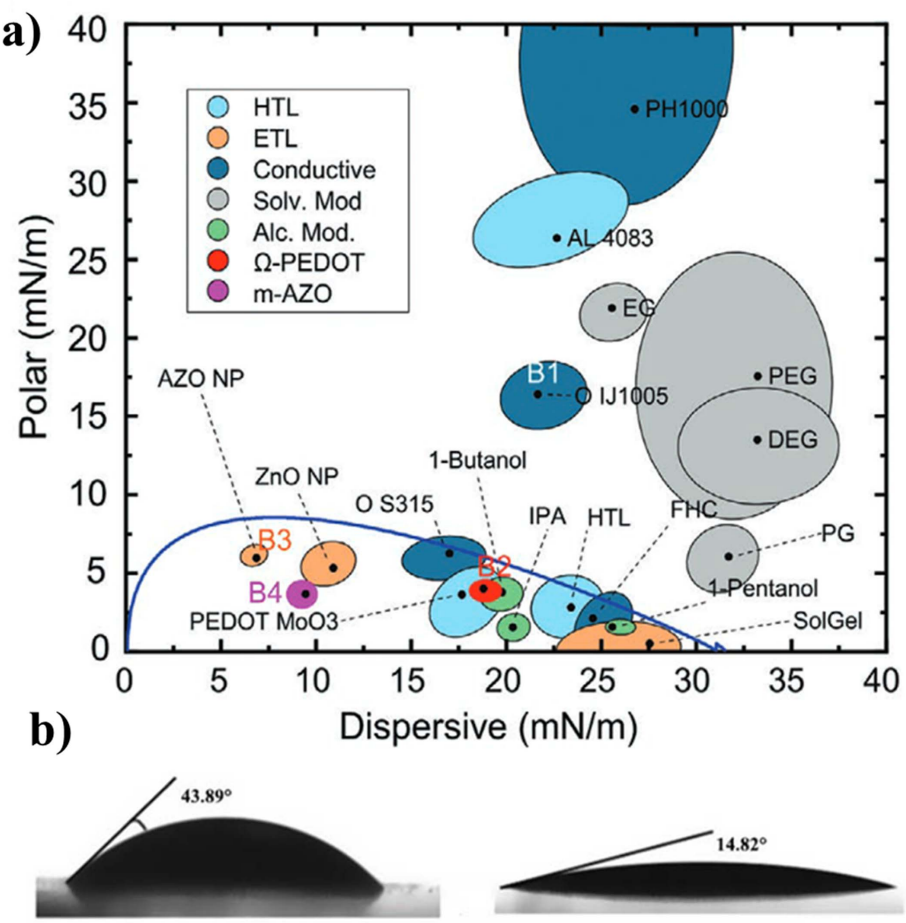

Figure 12. (a) Wetting envelope of the PTB7-Th:IEICO-4F (1:1) film placed against the liquid surface tension components of different HTL inks, ETL inks, conductive inks, and auxiliary solvents. [53] John Wiley & Sons. [© 2020 Wiley-VCH GmbH] (b) contact angle of PEDOT:PSS on glass substrates before plasma treatment (left), after plasma treatment (right). Reproduced from [136]. © IOP Publishing Ltd. All rights reserved.

inkjet-printing process compared with other high-throughput printing processes. Here, the constituents of the droplet including, e.g. solvents, polymeric species, or nanoparticles, have a strong impact on the quality of the inkjet-printed film.

The deposition pattern of functional materials is significantly influenced by the evaporation behavior of the droplet. Generally, there are three typical modes of droplet evaporation [138–140]: constant contact radius (CR) mode, constant CA mode, and stick-slip mode. In the CR mode, the droplet evaporates with a constant radius, and its CA decreases [140]. In the CA mode, the droplet maintains a constant CA, but the CR decreases [140]. In the stick-slip mode, the droplet initially evaporates in the CR mode until a certain CA is reached, after which the evaporation mode switches to the CA mode [138]. The CA and CR modes can be considered extreme cases of the stick-slip mode.

During evaporation, liquid molecules swiftly traverse the liquid surface, saturating the air just above the liquid droplet with vapor. If the surrounding air, far from the droplet surface, is not saturated, the vapor diffuses outward. If the characteristic time τ, representing the transfer rates of solvent molecules across the liquid/air interface, is much smaller than the vapor diffusion time, the droplet's evaporation is governed by the diffusive transport of vapor away from the droplet surface [141]. The vapor field can be approximately described by a quasi-static diffusion equation [141]:

$$\nabla^2 \times c = 0$$

where c is vapor concentration. The evaporative flux J is determined by the gradient in the vapor concentration and can be expressed as,

$$J = -D \times \nabla c$$

where D is the diffusion constant for vapor in air. Deegan *et al* [142] first proposed that the evaporation flux over a spherically capped droplet surface is not uniform but diverges at the edge for small CA. They demonstrated that the time evolution of droplet mass follows a power law. Hu and Larson [143], through a numerical model, derived an expression for the rate of mass loss, applicable only to droplets with a CA smaller than 90°. Popov [144] then developed a theoretical model of evaporation flux applicable to the full range

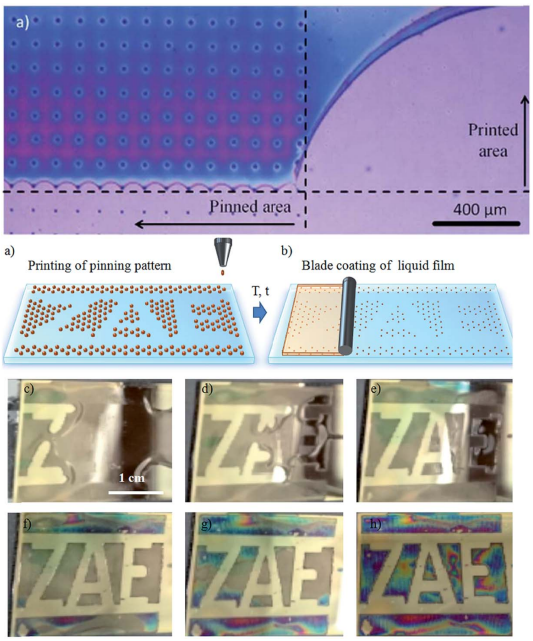

Figure 13. Top: optical microscope image of a dry PEDOT:PSS P Jet N V2 layer on a P3HT:PC60BM surface. The dashed and dotted lines mark the edges of the pinning and printing areas, respectively. Printing in an area covered by pinning centers results in stable film formation (left part). Printing on a blank surface results in dewetting and shrinkage of the layer (right part) [137]. Bottom: demonstration of pinning center approach for patterning of substrates. Reproduced from [137] with permission from the Royal Society of Chemistry.

of CA, later experimentally validated by Gelderblom *et al* [145].

Apart from the fluid dynamics, the characteristics (such as shape, wetting properties, and size) of the dispersed particles play a crucial role in the deposition process. Yunker *et al* [146] illustrated that ellipsoidal particles can mitigate the coffee-ring effect. This is attributed to the capillary interactions of ellipsoidal particles, which introduce a novel growth dynamics in particle deposition at the droplet's edge [147]. This mechanism prevents the self-pinning effect caused by the accumulation of particles at the droplet's edge. It is important to note that Yunker *et al* used hydrophobic ellipsoidal particles; however, for hydrophilic ellipsoidal particles, the deposition is not influenced by particle shape [148]. Recent research by Kim *et al* [149] emphasizes that the interplay between hydrodynamic force and capillary force in an evaporating droplet with ellipsoidal particles determines the resulting particle pattern. When dealing with spherical particles, a dot-like deposition pattern emerges when the particle size is sufficiently large, driven by capillary forces pushing particles inward [150–152]. In the investigation by Bhardwaj *et al* [153], the impact of particle-substrate Derjaguin–Landau–Vervey–Overbeek interactions on particle deposition is explored. Their findings reveal that an attractive particle-substrate interaction leads to a relatively thick and uniform deposit, while a repulsive interaction results in a ring-like deposit. Additionally, Bigioni *et al* [154] reported that drying a droplet with particles wetted at the fluid interface results in highly organized monolayer structures. The role of surfactants [155, 156] and substrate wettability in particle deposition is also discussed [157].

Following the pioneering work conducted by Deegan *et al* [142] on the coffee-ring effect, substantial advancements have been made in the modeling and simulation of macroscopic mass and momentum transport phenomena in drying droplets [144, 158, 159]. Despite this progress, there is a noticeable gap in the development of models and simulation methods that comprehensively address interfacial phenomena, contact-line dynamics, and deposition processes in drying droplets including drying colloidal suspension droplets. The existing theoretical models often rely on a convection-diffusion equation to describe the transport of colloidal particles [160, 161]. Unfortunately, these models fall short in capturing phenomena at the scale of individual particles, such as contact-line pinning, particle-particle interactions, and particle-substrate interactions. Xie *et al* [162, 163] conducted lattice Boltzmann simulations featuring fully resolved colloidal particles. This approach paves a path to comprehensively capture information at the scale of individual particles, providing valuable insights into the deposition process of functional layers in OPV inkjet printing, particularly in the presence of nanoparticles. Such simulations can be extended towards the effect of more complex shaped nanoparticles inside droplets or in the vicinity of interfaces and contact lines [164–170]. The above-mentioned theoretical investigations lead to several practical pathways to solve the coffee ring issue. As demonstrated in figure 14, during drying capillary flow causes the active part of the ink to flow towards the sides of the droplet resulting in thicker areas on the sides [142]. These can cause inhomogeneous layers especially with respect to surface topology, resulting in device defects and other issues with the functionality of the layer. The capillary flow can be overcome by the Marangoni flow [171]. In this case the coffee ring effect is either reduced or hindered. One approach to do this is increasing the evaporation rate by e.g. vacuum drying, additional air flow or higher temperature [172–174]. This is, however, not always possible, due to potential nozzle clogging if the hotplate heats up the printhead, or if there is no option to implement vacuum or gas flow. In this case, other options need to be used in order to prevent inhomogeneous drying. Ink formulation plays a crucial role here, as the boiling point and surface tension affect the coffee ring effect as well due to different drying kinetics and CA (figure 14). By using different boiling point solvents, special additives, or solvents with different surface tension, one can change the drying behavior and thus overcome the coffee ring

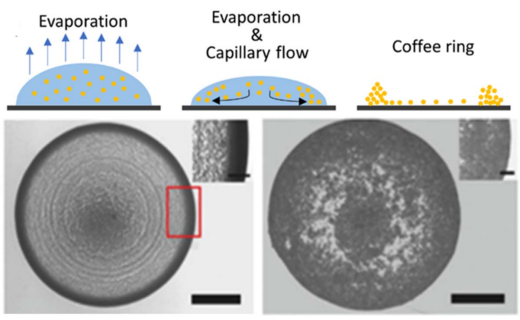

Figure 14. Schematic of the drying process and coffee ring effect (top) copyright under a creative commons license by Elsevier. Reproduced from [49]. CC BY 4.0, SEM images of printed GO ink droplets (bottom) left: clear coffee ring, right: uniformly dried deposit due to the marangoni effect. Reproduced from [181]. CC BY 4.0.

effect as well [175–179]. Furthermore, ternary solvent mixtures can enhance the Marangoni flow, what may lead to an enhanced molecular crystallization. On top, using different concentrations of active material inside the ink may also result in increased marangoni flow [81, 180, 181].

2.2.6. OPV active layer ink design for efficient inkjet-printed OSCs

All aforementioned challenges in OPV inkjet-printing as nano-morphology control, wetting, nozzle clogging and coffee ring effect are affected by the ink-requirements displayed in figure 3. Consequently, proper ink design is crucial for solar cell performance and later on for commercialization. As the most important layer of an OSC is the active layer, we will conclude this section with design rules for inkjet-printing inks on the example of an active layer.

Tables 4 and 5 list all parameters to be considered during ink and process design for getting good printing results. Following these design rules, one can create and optimize different kinds of inkjet-printed functional layers and overall OPV active layer films. Using a new system like PM6:Y6 in, e.g. OX that gives 15.6% for hot slot-die-coated layers at 110 °C [64], it is now possible to create a first idea of an inkjet-printed version of this solar cell. Printability and the nozzle clogging issue are improved by adding tetralin as high boiling point solvent with 1:1 ratio.

Additives may not be needed first, as wetting on top of ZnO is not an issue, but probably the polymer content may have to be increased to get suitable Reynolds numbers for proper drop formation. To produce proper nano-morphology, the main parameters to change are drying temperature and printing speed, as they change the drying time due to faster evaporation or thicker wet films. Optimizations for printing speed, drop spacing, and piezo pulses are necessary to get the best performance and most homogenous layer. Should performance or coffee ring effect be an issue during printing, additional changes of the ink like additives or changes in solvent ratios may solve the problem. The use of alternative solvent systems like CB:CN may be another solution.

2.3. Lifetime

Although reports on lifetimes of inkjet-printed solar cells are scarce, there is no reason to assume that they will fall short of those reported for OPV devices in general, which now have reached 11 000 h [183] in accelerated lifetime tests. Encapsulation techniques, such as lamination or thin film encapsulation, are applicable to inkjet-printed solar cells in the same way as they are for other emerging technologies. Even more desirable from the point of view of completely solution processed devices is the possibility to apply solution processed barriers against humidity and oxygen [184–186], either by coating techniques or, as demonstrated recently, by aerosol-jet printing [67]. It would be desirable to apply the encapsulation to inkjet-printed devices also by inkjet printing, especially in the case of delicate substrates and devices inkjet-printed onto 3D surfaces (see section 2.4.1).

2.4. Cost: upscaling and yield

Another prerequisite for successful commercialization is upscaling. The term upscaling is used in two different ways.

2.4.1. Towards large-area modules

On the one hand, upscaling refers to the production of devices with areas large enough to provide sufficient power output for potential applications. The first step in upscaling is the demonstration that inkjet printing of OPV on large areas is possible without significant power losses. At present, the record efficiency for 1 cm^2 inkjet-printed solar cell active layers is 12% [52]. However, further advances towards large-area devices with higher power without unnecessarily increasing resistive losses imply the transition from single cells to modules with serially interconnected cells [19], which will also provide higher voltages. Inkjet printing is perfectly suited for this task, as the required patterning is achieved by the very printing process, in contrast to coating techniques, which require an additional patterning step, e.g. laser ablation [19, 187]. One of the early works in which parts of OPV modules were inkjet-printed was published by Angmo *et al* who demonstrated the use of inkjet-printed silver grids as front electrode of organic solar modules [188]. Further progress was reported by Eggenhuisen *et al* who demonstrated 92 cm^2 P3HT:PC_{60}BM modules with 1.0% efficiency at a V_{oc} of 2.23 V (figure 15) [83]. The authors used electrical simulations to identify the high series resistance introduced by the molybdenum/aluminum/ molybdenum (MAM) bottom electrode as the cause of the relatively low fill factor of FF = 0.37. Further decreasing these resistive losses requires a module layout with

Table 4. Design rules for inkjet-printed OPV active layer ink design.

Ink compound	Benefits	Issues	Examples
Low boiling solvent <160 °C	→ Fast drying usually benefits nano-morphology and smooth surface topology [52] → Good solubility for active ink compounds → Usually good wettability as standard solvents for OPV	→ Fast evaporation leads to easy nozzle clogging → Usually Re numbers too high and not printable (splashing or no drop formation) [53] → Evaporation during drop ejection leads to aggregation before drop impact → Too fast drying may result in improper morphology and surface topology [182]	o-xylene CB
High boiling solvent >160 °C	→ Re numbers better suited for inkjet printing [53] → Low evaporation leads to less nozzle clogging and no evaporation before drop impact → Can fine tune drying process to achieve suitable morphologies [45]	→ Slow drying kinetics can lead to worse nano-morphology and surface topology [52] → May change wettability as non-standard additives → Different solubility may change aggregation processes → Different interaction para-meters towards active compound Changes thermo-dynamics of the system	Tetralin CN oDCB Mesitylene
Additive	→ Can influence wetting on previous top layer positively [53] → Can improve aggregation and phase separation towards a good morphology [75] → Can help to improve printability and reduce nozzle clogging [45] → Can reduce coffee ring effect	→ May influence printability due to Re number changes [53] → Can reduce device performance	DIO Indane Surfactants
Material concentration	→ Increases viscosity and thus changes Re number in order to change printability	→ May change aggregation behavior during drying → Leads to more probable nozzle clogging for higher concentration → Leads to faster gelation for higher concentration [45] → Can lead to preaggregation	

narrower cells. For modern active layer systems, cell widths should not exceed 4–8 mm, depending on the specific values of current density and electrode conductivity [40]. However, this causes two other serious drawbacks.

The first drawback concerns the reduced power output with respect to the total module area. With decreasing cell width (i.e. increasing cell number), the ratio of active to total module area, which is called GFF, decreases because the number of inactive interconnects between two adjacent cells increases. In the case of Eggenhuisen *et al* the module layout reduces the GFF to around 60%. In order to counterbalance this effect, the interconnect width must be reduced to a minimum [83]. By the combination of coating and laser patterning, interconnect widths of as little as 120 μm have been realized in OPV modules, yielding GFF of up to 98.5% [19, 189]. What is the highest GFF achievable in inkjet-printed modules? A simple geometric consideration provides an upper limit of the GFF. As can be deduced from figure 16, the smallest interconnect width possible is three pixels, as each of the three patterning lines P1, P2, and P3 needs at least one void pixel between adjacent cells to separate the electrodes and leave enough space for the contact between top and bottom electrode (usually, P2 widths of 20 μm are sufficient for achieving good electrical contact. However, in certain cases, e.g. AgNW/AgNW contacts, P2 widths of up to 140 μm are required) [32]. On top, also the size of a dried droplet need to be taken into account when planning resolution (figure 17). Figure 18 provides a plot of maximum GFF as a function of reciprocal pixel spacing, i.e. printing resolution, for three different cell widths. It shows that GFF values of 95% or more can be achieved if the appropriate printing resolution is applied. The minimum resolution is 120 dots-per-inch (DPI) for modules with 8 mm cells and 355 DPI for modules with 4 mm cells. The colored regions account for dry drop radii of n to (n + 0.5) times the pixel spacing where n is a natural number. No drop must be deposited at n pixels right and left of the

Table 5. Design rules for inkjet-printed OPV active layer process parameters.

Process parameter	Benefits	Issues	Work-arounds
Increased ink temperature	→ Increases solubility and changes aggregation behavior during drying → Reduce gelation processes[45]	→ Speed up solvent evaporation and lead to nozzle clogging → Need special care during printing to not change temperature during the process	Heated inkjet printheads with ink circulation
Increased substrate heating	→ Faster drying of droplets enhances fine nano-Morphology formation [52]	→ Fast drying results in inhomogeneous printing lines and Reduced vertical phase separation [52] → Substrate heating may induce solvent evaporation at the printhead and cause nozzle clogging	Optimization of temperature or separate drying step after printing
Drop spacing	→ Relevant to define wet film thickness, resolution and the formation of homogenous films [91]	→ Wrong choice leads to inhomogeneous films [91]	machine dependend parameter optimization
Printing speed	→ Can increase drying time and change nano-morphology formation process [89] → Can improve drying line issue[89]	→ Can lead to unfavorable nano-morphology [89] → Can lead to changes in drop volume for very high printing speeds [45]	Optimization needed
Printing piezo pulse	Defines[45] → Shape of droplet → Drop volume → Drop speed		Optimization needed

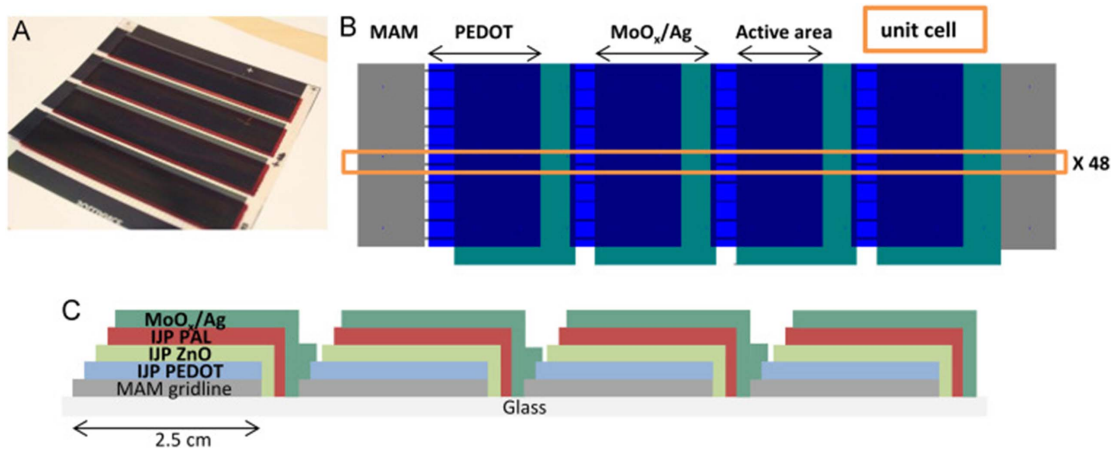

Figure 15. (A) Photograph of a module with three inkjet-printed layers, (B) schematic representation of modeled front electrode (molybdenum/aluminum/molybdenum (MAM) gridlines and busbars (gray) and inkjet-printed PEDOT (blue)) and back electrode (MoOx/Ag (teal). (C) Cross section of a single gridline in 4 adjacent cells. Reprinted from [83], Copyright (2015), with permission from Elsevier.

actual P(1/2/3)-line (in addition to the not-printed centered pixel). For a drop radius of n times pixel spacing, this leads to a void of 2 times the pixel spacing. For a drop radius of n + 0.5 times pixel spacing, this leads to a void of 1 time the pixel spacing.

Dry drop diameters may vary significantly, mainly depending on the volume of the ejected drop, but also on the nature of ink and substrate, as shown in figure 17(a). For the same drop volume of 30 pL, dry drop diameters between 96 μm for the active layer ink, and 324 μm for the Ag nanoparticle ink, are obtained. An approximate upper limit of dry drop diameter can be obtained by the following considerations.

The sizes of liquid drops after impact on the surface are mainly determined by the volume of the ejected drop, drop velocity, drop deformation upon impact and the surface tensions of ink and substrate.

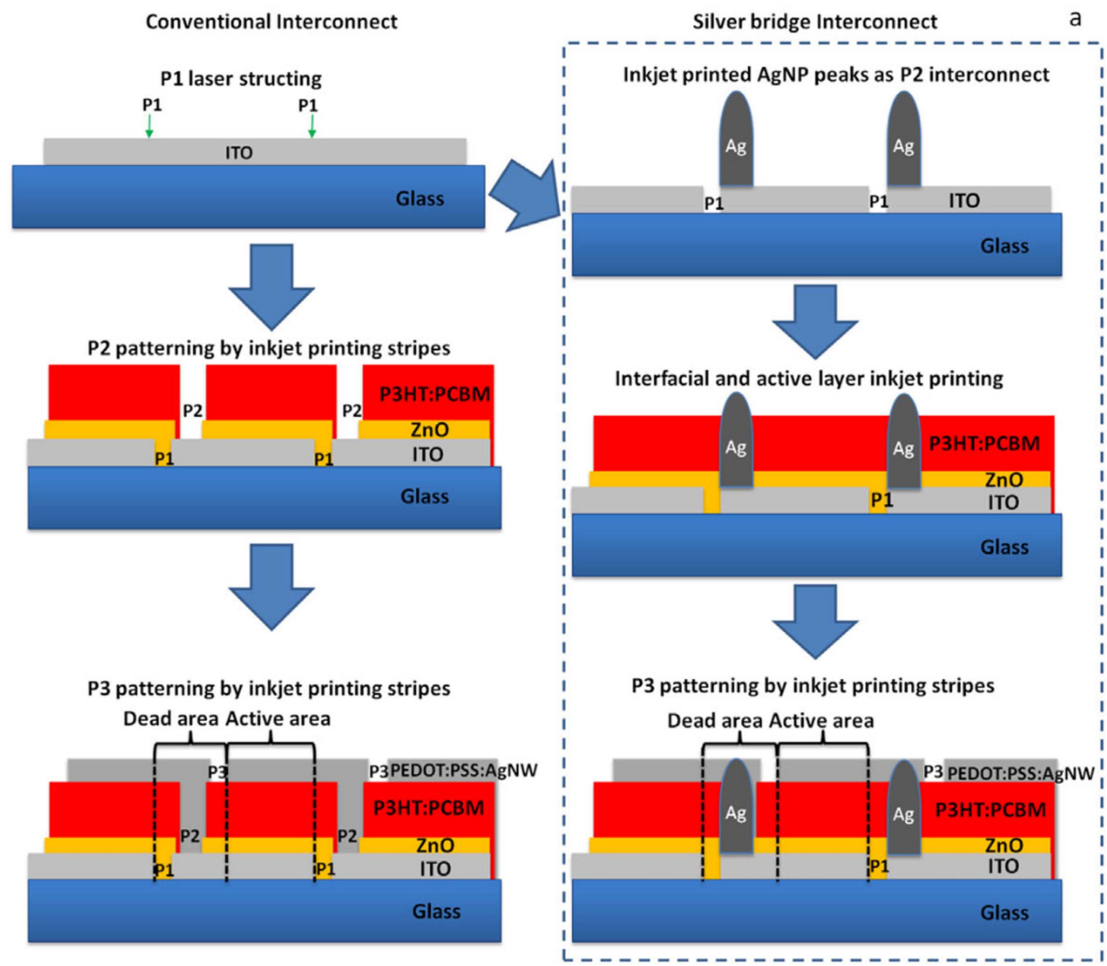

Figure 16. Schematic illustration of organic solar module fabricated by inkjet printing method. In conventional gap layout, interconnection is achieved by introducing a gap during the active and interlayer printing process so that the top electrode can diffuse into the gap and form a connection with the bottom electrode. The novel bridge interconnect proposed in this work is highlighted in blue dashed bracket. AgNP lines are printed so that the top and bottom electrode can be bridged at the interconnection area. [187] John Wiley & Sons. [© 2018 WILEY-VCH Verlag GmbH & Co. KGaA, Weinheim].

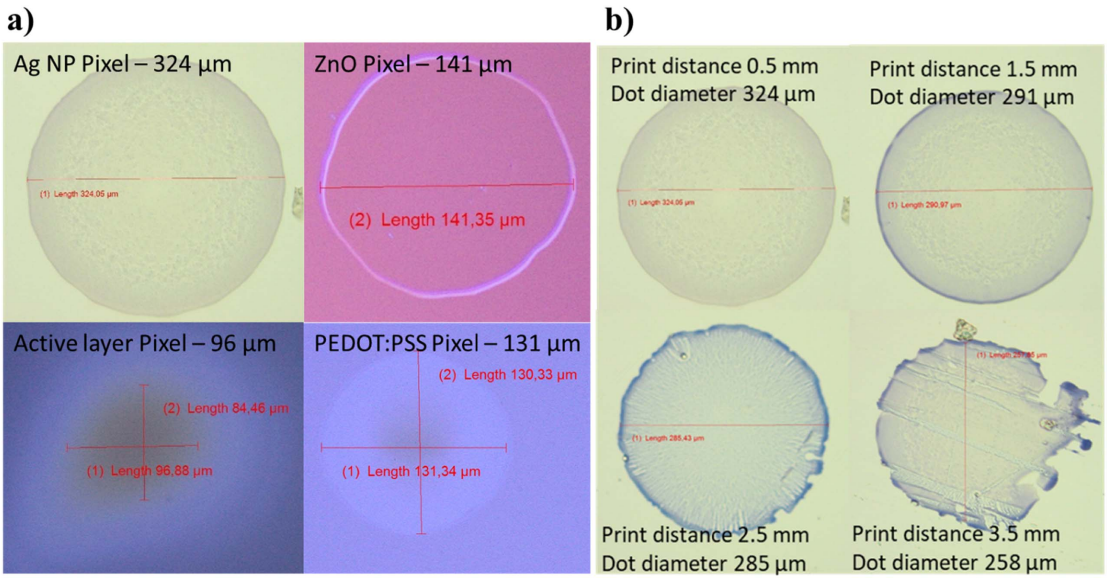

Figure 17. (a) Micrographs of dry drops of different inks deposited with a Spectra SE print head (ejected drop volume = 30 pL). AgNP on PEDOT:PSS, ZnO NP/solvent on ITO, P3HT:PC60BM/xylene on ZnO, PEDOT:PSS/water on P3HT:PC60BM [68]. (b) Microscope images of AgNP dots inkjet-printed with different distances between nozzle and substrate. Reproduced from [68]. © The Author(s). Published by IOP Publishing Ltd. CC BY 4.0.

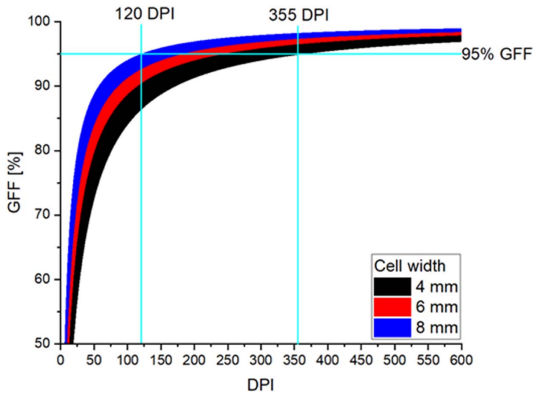

Figure 18. Dependence of geometric fill factor (GFF) of inkjetprinted solar modules on printing resolution.

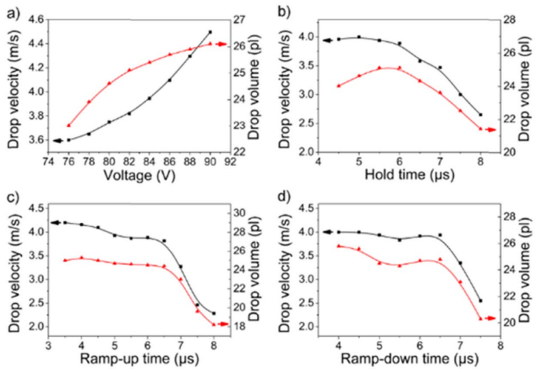

Figure 19. Drop velocity and drop volume measurements for different jetting parameters. Reproduced with permission from [45].

Modern standard printheads provide drop volumes ranging from 1.5 to 200 picolitres [69], which can be modified by up to 30% using appropriate piezo pulses (see figure 19) [45]. The calculation of drop sizes is a complex topic, and several methods for assessing them have been proposed [51, 174, 190]. For the sake of simplicity, we assume that the drop of diameter D_0 spreads on the surface, i.e. upon impact, the drop of diameter D_0 is deformed and the drop diameter increases to r_{max}. Given by the tanner equation, the contact line advances until the equilibrium CA Θ is reached. The resulting drop diameter is then given by equations (4) and (5):

$$\boldsymbol{D} = \boldsymbol{\beta} \cdot \boldsymbol{D_0} \tag{4}$$

$$\beta = \sqrt[3]{\frac{8}{\tan(\theta/2)\left(3+\tan^2(\theta/2)\right)}} \tag{5}$$

Possible overspreading of the drop with subsequent contact line pinning has been accounted for by empirical correction factors [174]. The diameter of the drop after drying will be equal to D if the contact line remains pinned during the evaporation of the solvent, while it will be less otherwise (see section 2.2.5). Another important factor for drop impact and resolution is the distance of the printhead from the substrate. It is one of the main benefits of a non-contact technology that there is a gap between the printhead and the substrate as it guarantees that there is no damaging of the surface, thus enabling more versatile surfaces as substrates. However, if the gap exceeds a certain distance, in the example of AgNP ink around 2.5 mm (figure 17(b)), the resulting droplet will decrease in size, as a consequence of solvent drying during flying, and will lose its round shape as agglomerates will already form during drying in air. This undesired effect is ink-dependent and can be solved by proper distance or changes in, e.g. the volume fraction of high boiling solvent.

During the drying process, the contact line either remains pinned (CR-constant contact line radius) or recedes to keep the CA constant (CA-constant CA). Also, intermediate cases, the stick-slip mode and the stick-jump mode are observed. Although the phenomenon of CA hysteresis has been the subject of numerous experimental and theoretical investigations, it is still not fully understood. Inks containing surfactants or loaded with particles tend towards contact line pinning.

The above estimate of maximum achievable GFF is an upper limit and may be compromised by several factors. In a real production process, registration of the subsequent layers with sufficient accuracy is required, which is non-trivial if the devices have to be removed from the printer between two subsequent layers for post-treatment. Maisch *et al* have demonstrated that registration between layers is possible on R2R equipment with accuracies of 100 μm or better (see section 2.3.2) [45]. Another prerequisite for reaching high values of GFF is a perfect printing pattern. Any deviation from perfectly straight lines will cause additional losses. In the worst case, bulging of the lines will lead to short circuits between the bottom or top electrodes of adjacent cells (figure 20(a)). Stringer and Derby [191] proposed equation (6) for assessing the critical drop spacing, where ß is calculated from equation (5),

$$p_{crit} = \frac{2\pi\,\Delta_0}{3\beta^2\left(\frac{\theta}{\sin^2\theta} - \frac{\cos\theta}{\sin\theta}\right)} \tag{6}$$

Scalloping is observed for $p > p_{crit}$. For $p < p_{crit}/1.5$ the line is prone to bulging. Soltman and Subramanian extended this concept by including also the delay between nozzle firing (figure 20) [172] to account for the drying of the droplets [174]. Soltman extended this concept to 2D film formation [174]. Chen *et al* found an optimal drop spacing of 40 μm for PBDB-T:ITIC films [91].

Another downside of modularization, i.e. the separation of large area devices into cells, is the resulting multitude of interconnects, which are quite conspicuous if prepared in the traditional way, which is detrimental for optically attractive modules. Maisch *et al*

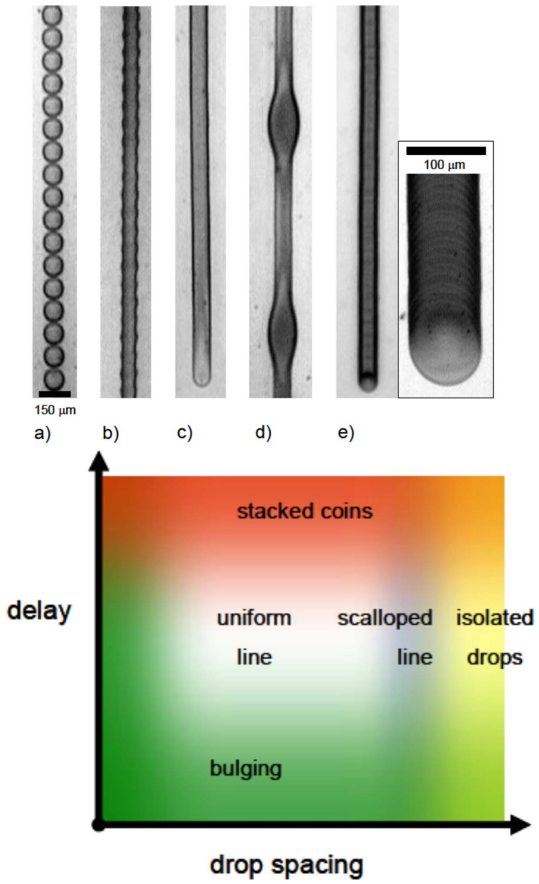

Figure 20. Dependence of line shape and drop spacing and delay (a) individual drops, (b) scalloped, (c) uniform, (d) bulging, and (e) stacked coins. Drop spacing decreases from left to right. Reprinted with permission from [172]. Copyright (2008) American Chemical Society.

have made use of inkjet printing to realize a novel concept of 'shy', i.e. inconspicuous interconnects, which relies on printed silver lines (figure 16) and can further increase the GFF [187]. The concept was demonstrated by inkjet printing a 2.5 cm^2 large P3HT:PC60BM based module, consisting of three cells in series, with an efficiency of around 2.8%, which is only 10% less than that of a single lab cell. More recently, the same authors have reported R2R inkjet-printed flexible 3-cell solar modules with a PCE of 4.7% on an active area of 10 cm^2, based on the active layer system PV2000:PC71BM (figure 21) [45].

There are other concepts to achieve even higher GFF. One for interconnect formation in thin film PV which employs the combination of laser patterning and inkjet-printing, the so-called OSI process, was suggested by Crozier *et al* [192]. First, all layers are deposited to form the complete cell structure, then three laser scribes are written simultaneously. Scribe A removes the entire stack to the glass, resulting in electrical isolation of the front contact. Scribe B and P3 stop on the transparent conductor: one exposes the front contact for electrical connection and the other isolates the back contact. Two inkjet heads follow, the first fills in scribe A with an insulative material and the second prints a metallic bridge between the front contact of one cell and the back contact of the adjacent cell. This concept is of industrial relevance as it helps to reduce the cost for manufacturing of modules with free form patterns by decoupling the layer deposition processes from the patterning processes. This allows patterning of prefabricated semi-finished standard modules at a later time, according to a certain customized module layout.

2.4.2. Toward high throughput manufacturing

On the other hand, the second meaning of upscaling refers to increasing the throughput of production to industrial scale, which is essential to bring costs down to acceptable levels.

The cost of production is composed of the bill of materials (BOM), investment and operation. The BOM is obtained from material cost per gram, material required for 1 sqm module area, fraction of material not wasted, and production yield. While material waste is around 90% for spin coating, it is close to zero for inkjet printing. On the other hand, nozzle clogging may be a serious problem for inkjet printing, as it can reduce the production yield substantially.

Many authors have speculated about industrial application of inkjet technology in OPV [71, 193], but only few have really demonstrated the capability [188, 194]. With increasing printed area, the processing complexity increases. Larger areas require a substantial number of print heads with hundreds or thousands of nozzles in total. This leads to a rising probability of nozzle clogging and consequent printing defects. Furthermore, ink sedimentation becomes a serious issue as production runs become longer. Both nozzle clogging and sedimentation can be reduced by implementing ink circulation systems [51, 69]. In parallel, advanced ink formulations offering increased stability against sedimentation and gel formation must be developed.

To compensate for investment cost, high throughput production is necessary, which is provided by R2R printing at low operational cost.

A high-speed R2R inkjet process for manufacturing OPV modules has been developed by P. Maisch [45]. The printing machine, assembled by DURST Austria GmbH, consists of four printing stations, each of which carries four SAMBA print heads, thus enabling a printing width of 17.2 cm. The substrate is a PET loop of 7–8 m in length and up to 20 cm in width, which runs over three rollers, controlled by a web-guide. The maximum web speed for stable operation is around 40 m/s. The printing stations are coordinated by a controller, using the input of an encoder reel, which allows printing consecutive layers with a registration precision of 100 μm. Continuous circulation of the ink reduces nozzle clogging. Several heating stations provide rapid drying of the deposited ink. Using this

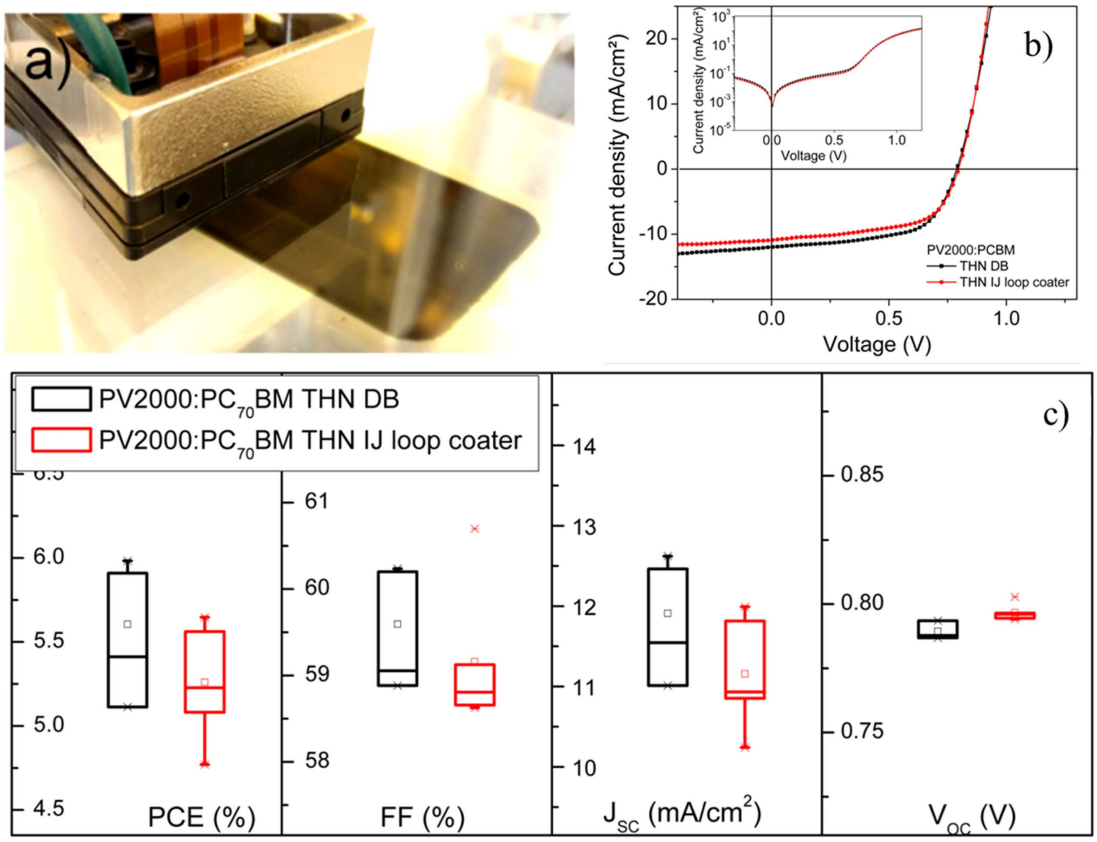

Figure 21. (a) Printing process of homogeneous PV2000:PC70BM layers from THN ink with the single pass inkjet (b) Representative current-voltage characteristics of solar cells with PV2000:PC70BM active layers doctor bladed (black) and printed at the single pass loop coater (red) from THN based ink. The inset shows the current-voltage characteristics measured in the dark. (c) Box plot performance comparison of PV2000:PC70BM solar cells with blade coated (black) and inkjet-printed (red) active layer from THN ink. Each box contains data of at least five solar cells. Reproduced with permission from [45].

machine, fully inkjet-printed devices of the structure AgNW:ZnO/PV2000:$PC_{70}BM$/AgNW:PEDOT:PSS were fabricated. In order to speed up the production process, the number of printing steps was reduced from five to three by printing mixtures of AgNWs with ZnO nanoparticles in 1-pentanol or with PEDOT:PSS for bottom and top electrodes, respectively. For the active layer, homogeneous and defect free layers of PV2000:$PC_{70}BM$ were printed by applying inkjet inks based on pristine THN, resulting in a device efficiency of 5.2% for single cells, which is in the same range as those obtained for doctor bladed active layers (figure 21). Finally, fully inkjet-printed flexible 3-cell solar modules with a PCE of 4.7% on an active area of 10 cm^2 were demonstrated (figure 22).

2.4.3. Production yield: nozzle clogging

Typical nozzle sizes of commercial inkjet printheads are in the range of 30–60 μm and use resolutions of 100–1200 DPI and drop volumes between 6–200 picolitre [195]. For OPV applications a typical print head is the Dimatix Spectra SE print head using a nozzle diameter of 35 μm with 25–30 picolitre drop sizes and an intrinsic resolution of 50 DPI that can be increased up to 1000 DPI by printhead tilting. As these small picolitre droplets show a very high surface to volume ratio, drying effects need to be considered while inkjet printing. Too fast drying can result in aggregations that are formed within or at the nozzle of the printhead, resulting in either bad or not working nozzles and thus directly influence the printed layer as shown in figure 23. Inhomogeneities or missing lines can be consequences of clogged nozzles leading directly to bad or non-functional devices.

Especially for upscaling this is a critical issue as many consecutive printheads with thousands of nozzles contribute to one functional device. The main parameters that influence this issue are the boiling point of the ink solvent and the temperature of the ink while jetting. Another issue is the behavior of the active components in the ink. These may be nanoparticles, polymers or other components that will define the dry film properties. Polymer solutions at different temperatures and concentrations are either fully dissolved or form particles or gels, that would lead to nozzle clogging. A low boiling point solvent-if printable-results in very fast drying even at room temperature, leading to fast clogging of the nozzles as the solvent evaporates during the jetting. Consequently, a high boiling point solvent is always necessary to

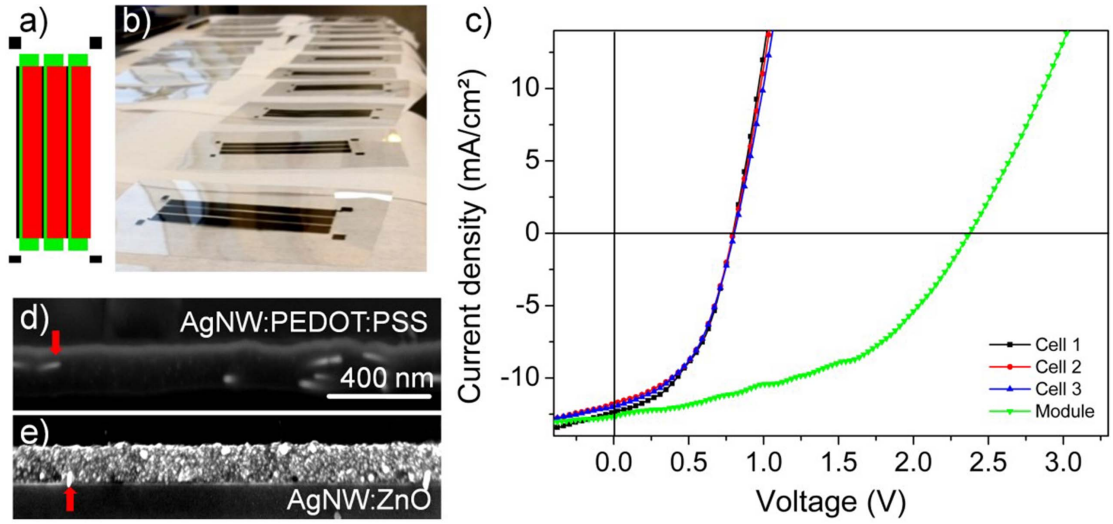

Figure 22. (a) Layout of fully inkjet-printed 10 cm^2 three-layer modules, black: AgNW:ZnO base electrode, green: PV2000:PC70BM active layer, red: AgNW:PEDOT:PSS top electrode. (b) Photograph of fabricated modules. (c) J–V characteristics of PV2000:PC70BM three-layer solar module and single module cells. (d) SEM cross section image of an inkjet-printed AgNW:PEDOT:PSS blend electrode and e) inkjet-printed AgNW:ZnO blend electrode. The red arrows point at the AgNWs, which appear brighter compared to the matrix material. Reproduced with permission from [45].

realize long-term stable inks that do not form a gel at least for several hours. P. Maisch developed an OX:tetralin ink where 20 mg/ml P3HT/PC60BM were still liquid after 4.5 h [45]. Finally, the choice of the appropriate printhead may help to reduce nozzle clogging, as demonstrated in figure 23. While the PV2000:PC71BM ink caused serious nozzle clogging of the Samba printhead (drop volume 2.4–10 pl), almost perfect printing patterns were achieved with the Spectra SE printhead (nozzle diameter 35 μm-30 pl). Additional factors for commercialization are the suitability of the inkjet printhead for non-polar solvents and proper ink storage stability.

While commercially available printheads already show a very broad range of chemical stability [196], the ink's storage stability is another topic to be considered during ink formulation. The stability is influenced by several factors like solubility in the respective solvent, aggregation behavior of the dissolved material, reactions due to heat, light, oxygen and temperature [45]. Usually the ink's storage stability can be enhanced by storage in cool and dark places under inert atmosphere. For nanoparticle inks, especially the electrode materials like silver nanoparticles and nanowires, the main issue is the aggregation during storage and subsequent sedimentation. These topics are usually addressed by ink manufacturers that use steric or electrostatic stabilization to slow down agglomeration [197]. Besides proper ink storage, preprocessing steps, such as mixing, heating, ultrasonication or filtering, immediately before use serve to prolong the shelf life of inks towards month or even years [45]. For active layer inks, storage is even more critical, as these materials are prone to reaction with ambient oxygen. Here storing under nitrogen atmosphere in the dark is optimal but not always possible. This topic is mainly material related and part of current research in active layer synthesis. One approach reported by Steinberger *et al* is the use of stabilizing additives that prevent oxidation even upon exposure to high temperatures for over 24 h [198]. During printing one needs to address additionally the sedimentation of particle inks in the printer. Here a constant recirculation is necessary to overcome that issue. More information is provided in the review by Kwon *et al* [69].

2.5. Potential niche markets

2.5.1. Direct functionalization of 3D objects by inkjet printing

Recently, the advent of the IoT technology has created a potential new application for inkjet printing of PV devices. It is estimated that the global IoT market size will be 1.55 trillion USD in 2026, up from 749 billion USD in 2020, with an annual growth rate of 12.20% [199]. The fast-expanding market triggers a dramatic increase in the number of devices, which is predicted to exceed 30 billion by 2025 according to a statistical analysis [200]. Assuming a 3 year life span of the batteries powering these devices, over 27 million batteries would have to be changed every day. As battery change requires manpower it is costly, which makes powering by light harvesting an attractive option. Printing the required PV devices directly on the housing of the IoT devices represents a cost-efficient alternative to the attachment of solar panels. Consequently, manufacturing of fully inkjet-printed 3D integrated electronic devices has received increasing attention, even more so as the resulting techniques

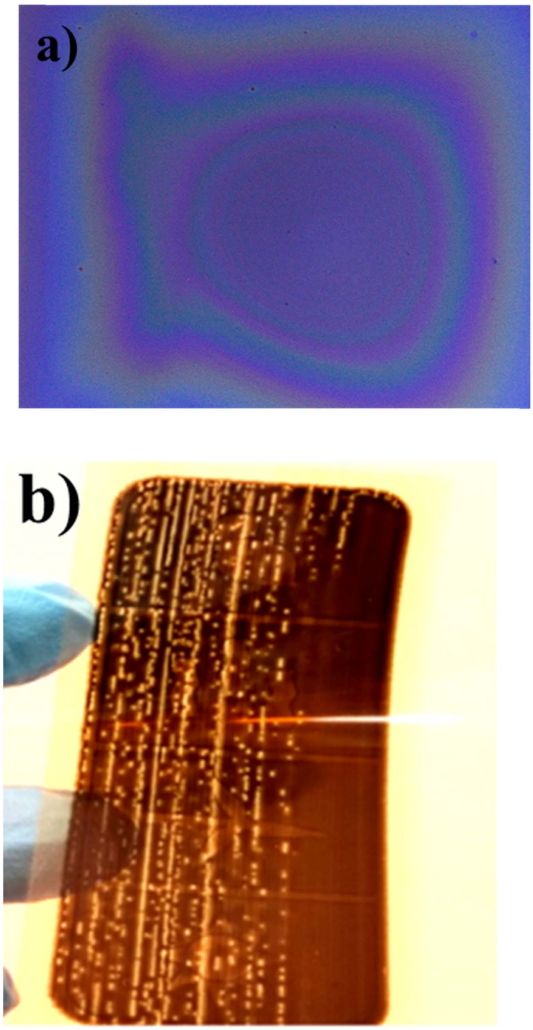

Figure 23. (a) Compatibility of ink (PV2000:PC60BM) and printhead (Spectra SE): defect-free film (b) incompatiblility of ink (PV2000:PC71BM) and print head (Samba): active layer with defects due to nozzle clogging. Reproduced with permission from [45].

can be directly transferred to the printing of OLEDS on automotive parts [49].

For inkjet printing on 3D substrates a special inkjet printer was built by Steinberger *et al* A 5-axis robot system was equipped with a Spectra S-class inkjet print head, controlled by Meteor software and hardware. The speed of the different axes was transformed into transistor-transistor logic signals that feed the printing software with the required printing frequency according to the resolution in printing direction, while resolution vertical to the printing direction was adjusted by tilting the printhead. Complex 5-axis movements were then programmed in Motion 3D using CAD drawings of the respective object to print on (figure 24) [68].

The corresponding process for inkjet printing organic electronic devices on 3D objects was developed by systematically investigating the influence of printing distance and angle on the functional layers. Printing of OSCs onto a 3D object with glass/ITO surfaces has been shown to result in high PCE's of up to 6.5%, even for high inclination angles of 60° between print head and substrate. Complete inkjet printing of the whole solar cell stack including a AgNP bottom electrode onto a 3D object was also achieved and yielded PCE values of up to ∼3% (figure 25). In this case, gravity induced material flow of the AgNP ink on tilted surfaces and the resulting bottom electrode roughness were found to limit device performance [201]. Once this open challenge is overcome, e.g. by further improving the ink formulation or by in-situ curing of the ink, inkjet printing of highly efficient solar cells directly onto 3D objects will be an attractive option for powering surfaces of any kind.

2.5.2. Design

Probably the strongest selling point of inkjet-printed OPV is the ability to create PV devices of almost discretionary forms and shapes (figure 26). Ample use of this ability to create devices of superior optical appearance has been made by several groups, exemplified by the designs presented in figure 27 [45, 84, 88]. In most cases, each design consists of a single cell, which often leads to compromised performance, due to the relatively large series resistance of the electrodes. In order to improve performance, the figure has to be divided into several cells, which then may be connected in series or parallel. However, this will lead to less appealing designs due to conspicuous circuitry. This can be avoided by either making the interconnects part of the design (figure 26) or by making them inconspicuous. The latter strategy was adopted by Tam *et al* who combined the concept of 'shy' interconnects (figure 26) with invisible AgNW electrodes to create a semitransparent PV portrait, consisting of 10 serially connected P3HT:PC60BM based solar cells with a total power output of around 0.5 Wp, which is sufficient for driving a digital clock (figure 25) [187].

One of the key advantages of inkjet-printed OSC's is the possibility to print different active layers and thus different colors in a well-defined way onto different parts of the same substrate. Although there has been no report on such multi-colored organic solar modules so far, organic solar modules with different colors have been realized in different ways (figure 27). While Sang *et al* used a bluish camouflage design of their OSC [52], Maisch *et al* used a special epoxy glue for coloration. During encapsulation the UV-curable epoxy glue (Katiobond LP 655) dissolved the PC70BM in areas which were not protected by the top electrode, thereby changing the color of the active layer in the semitransparent devices from brown to green [45].

2.5.3. Power-to-weight ratio

Integration into textiles or air- and space crafts, where ultra-high flexibility and ultra-low weight are required, are rapidly evolving fields of OPV

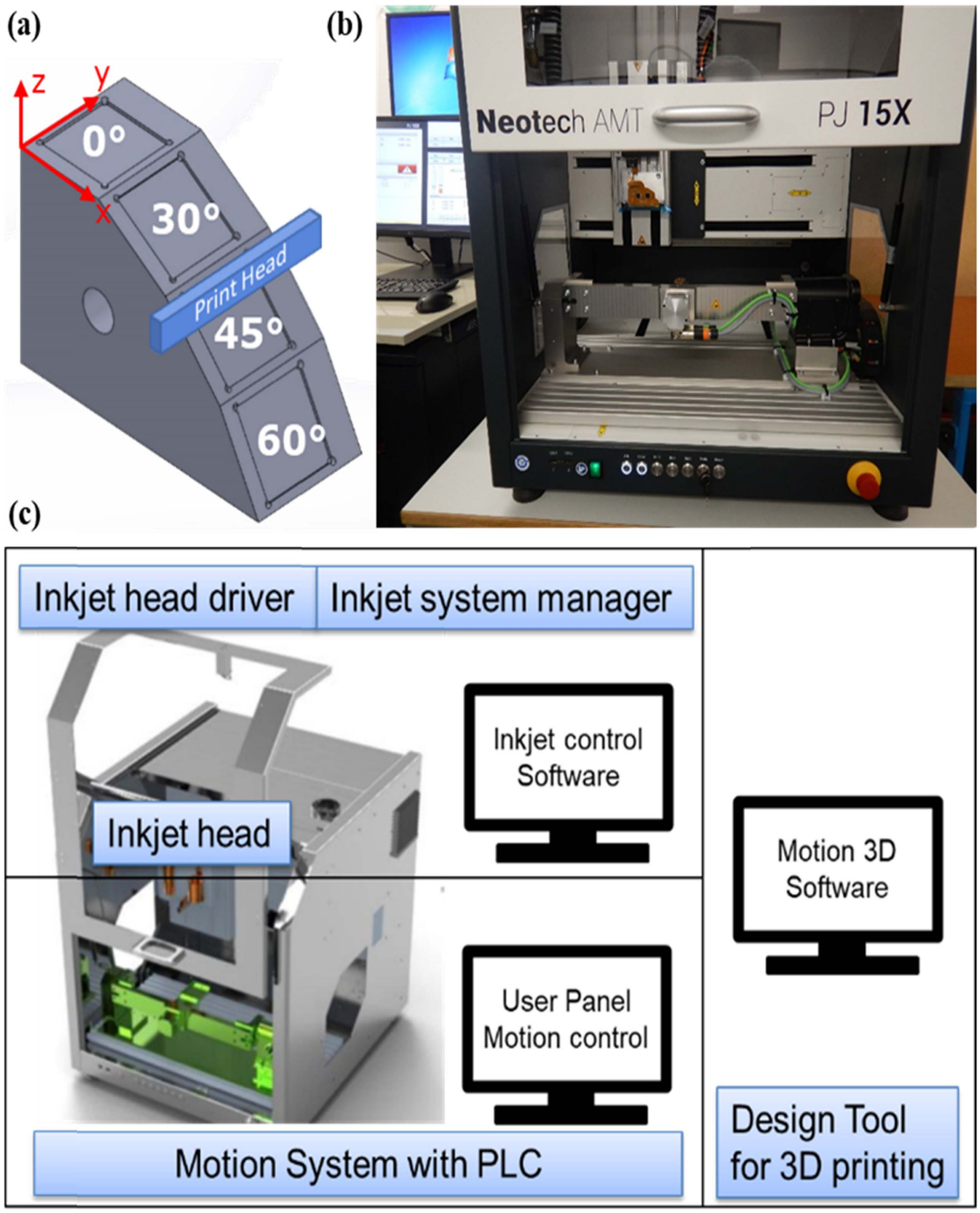

Figure 24. (A) 3D object holder with inkjet printing unit above. (B) 5-axis robotic system with inkjet printing unit. (C) Schematic of the 3D inkjet printing control units. Reproduced from [68]. © The Author(s). Published by IOP Publishing Ltd. CC BY 4.0.

[202–207]. Bihar *et al* have demonstrated inkjet-printed ultra-lightweight OSCs on parylene using PEDOT:PSS electrodes (figure 28) [46]. Power-to-weight ratios as high as 6 W g^{-1} were reached which is one magnitude higher than comparable poly-Si solar cells or triple junction GaAs solar cells. Although ultra-lightweight printed electronics have also been manufactured by other printing and coating methods[208, 209], inkjet printing is the preferred technology for this application, because as a non-contact printing method it allows the manufacturing of OPV modules without damaging the ultrasensitive substrates, neither by the deposition of the layers nor by the patterning processes.

3. Conclusion and Outlook

In terms of PCE of small research cells, inkjet printing of OSCs has almost closed the gap to other industrially relevant deposition techniques, such as flexographic printing and slot die coating. Considering the boundary conditions of industrial ink jet printing as illustrated in figure 3, closing the remaining gap will be mainly the task of ink engineering, preferably

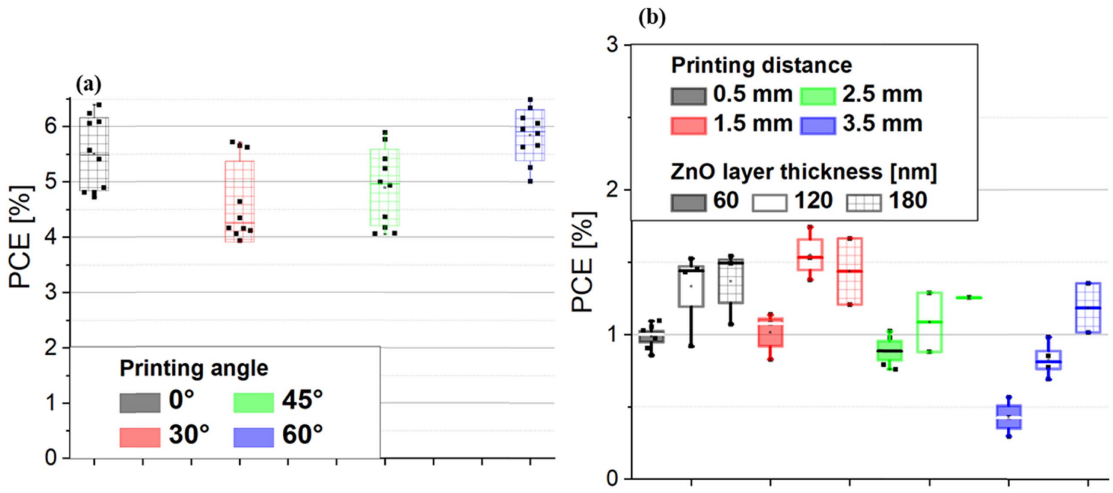

Figure 25. (a) 3D inkjet-printed solar cells on glass/ITO substrates with the layer stack ZnO/PV2000:PC60BM/PEDOT:PSS/AgNW using different printing angles between print head and substrate. (B) Power conversion efficiencies of all inkjet-printed solar cells on glass substrates with the layer stack AgNP/ZnO/PV2000:PC60BM/PEDOT:PSS/AgNW having different layer thicknesses of ZnO and having been printed with different distances between print head and substrate. Reproduced from [68].

Figure 26. Inkjet-printed photovoltaic portrait of Alan Heeger, consisting of 10 solar cells connected in series. Reproduced with permission of P Maisch.

based on a better understanding of the formation of bulk heterojunction morphologies for modern high efficiency materials. On the level of large area modules, which are required for 'real world' applications, there is still a substantial gap to the state of the art of 'printed' organic PV, which is currently defined by slot die coating. However, the most recent developments in transferring research type OSCs to OPV modules show that ink jet printing cannot only reach comparable efficiencies also on large areas, but it can also achieve competitive GFF. In contrast to coating techniques, ink jet printing does not require additional patterning equipment, which saves on capex and enables a more robust production process, e.g. for the manufacturing of tandem modules. In terms of cost, ink jet printing has to compete mainly with slot die coating, which in combination with in-line patterning techniques has the advantage of higher throughput at the same capex.

In terms of market opportunities, the unique capabilities of ink jet printing open up a wide range of attractive industrial applications, not only of printed PV, but of printed electronics in general. One of these capabilities is in-process patterning, which enables the production of discretionary shapes and patterns with extremely short setup times. This allows not only the manufacturing of building-integrated photovoltaics installations and consumer PV gadgets with attractive designs, but also the realization of novel PV concepts, such as lateral multi-junction devices [210]. Another unique feature of ink jet printing is its contactless nature, which enables printing of optoelectronic functionalities on discretionary, delicate or even 3-dimensional surfaces. This will be highly attractive for the automotive industry, as LEDs, sensors, or energy sources may be printed directly on car bodies. Printing solar modules directly on the hulls of air or space craft will result

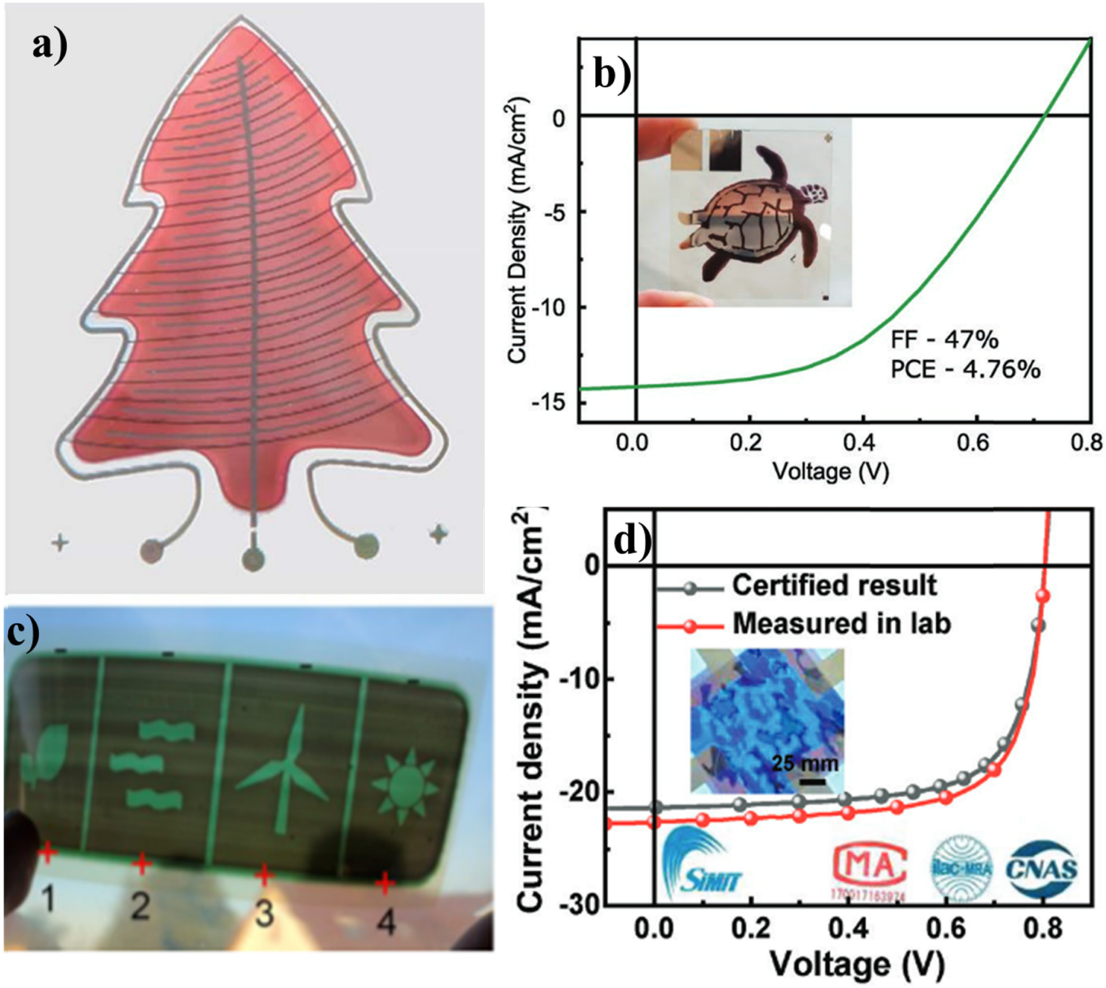

Figure 27. Different colored inkjet-printed OSC's; (a) red christmas tree. Reproduced from [84]. CC BY 3.0. (b) printed turtle. [88] John Wiley & Sons. [© 2019 WILEY-VCH Verlag GmbH & Co. KGaA, Weinheime] (c) printed and UV cured active layer. Reproduced with permission from [45]. (d) camouflage pattern due to different active layer thicknesses. [52] John Wiley & Sons. [© 2023 Wiley-VCH GmbH].

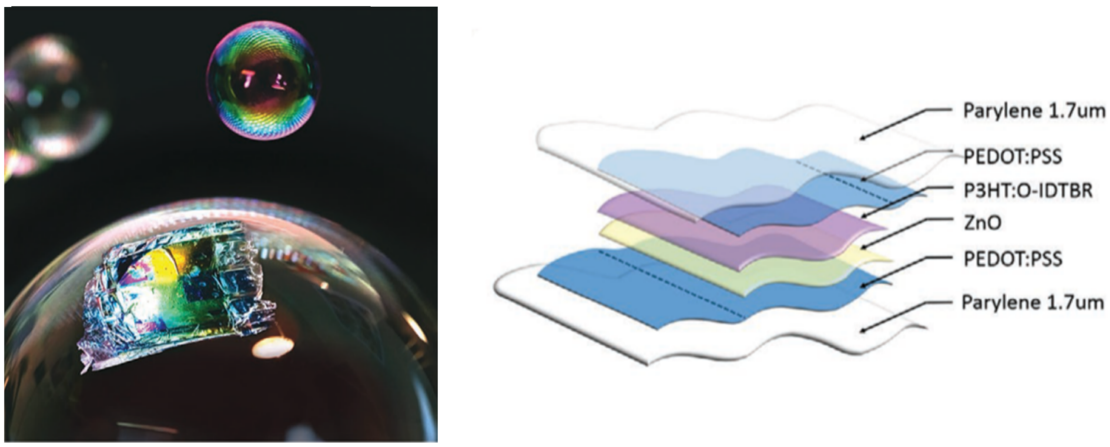

Figure 28. Photograph of ultralight inkjet-printed organic solar cells embedded in a soap bubble (left); schematic view of layer-by-layer composition of the solar cell (right) reproduced from Bihar *et al* with permission from Advanced Material Technologies. [46] John Wiley & Sons. [© 2020 WILEY-VCH Verlag GmbH & Co. KGaA, Weinheim].

in unrivaled power-to-weight ratios, while printing organic solar modules directly on façade elements or shading lamella will provide PV installations with discretionary patterns, without significantly increasing the fire load.

Data availability statement

No new data were created or analysed in this study.

Acknowledgments

The authors acknowledge the 'Solar Factory of the Future' as part of the Energy Campus Nuremberg (EnCN), which is supported by the Bavarian State Government (FKZ 20.2-3410.5-4-5). H-J E and C J B acknowledge funding from the European Union's Horizon 2020 INFRAIA program under Grant Agreement No. 101008701 ('EMERGE'). Part of this work has been supported by the Helmholtz Association in the framework of the innovation platform 'Solar TAP'. M S, C J B, J H, and O R acknowledge the DFG project 'Prozess-Struktur Relationen für die lösungsmittel-basierte organische Photovoltaik' (GZ: BR 4031/20-1) for financial support.

ORCID iDs

Marc Steinberger https://orcid.org/0000-0002-1558-9415
Olivier J J Ronsin https://orcid.org/0000-0002-3958-8636
Jens Harting https://orcid.org/0000-0002-9200-6623
Christoph J Brabec https://orcid.org/0000-0002-9440-0253
Hans-Joachim Egelhaaf https://orcid.org/0000-0002-8263-8125

References

[1] Ritchie H, Rosado P and Roser M 2024 *Energy Production and Consumption* Our World in Data (available at: https://ourworldindata.org/energy-production-consumption) (Accessed 6 February 2024)
[2] Bonnassieux Y *et al* 2021 The 2021 flexible and printed electronics roadmap *Flex. Print. Electron.* **6** 023001
[3] Forberich K, Guo F, Bronnbauer C and Brabec C J 2015 Efficiency limits and color of semitransparent organic solar cells for application in building-integrated photovoltaics *Energy Technol.* **3** 1051–8
[4] Lucera L 2016 Closing the efficiency gap between lab-produced organic solar cells and roll-to-roll printed modules *Doctoral Thesis* Friedrich-Alexander-Universität Erlangen-Nürnberg
[5] National Renewable Energy Laboratory 2023 *Best Research-Cell Efficiency Chart* (available at: www.nrel.gov/pv/cell-efficiency.html) (Accessed 19 December 2023)
[6] Xu Y *et al* 2023 Recent progress in all-solution-processed organic solar cells *Chin. J. Chem.* **42** 190–98
[7] National Renewable Energy Laboratory 2023 *Champion Photovoltaic Module Efficiency Chart* (available at: www.nrel.gov/pv/module-efficiency.html) (Accessed 19 December 2023)
[8] Pang B, Liao C, Xu X, Yu L, Li R and Peng Q 2023 Benzo[d]thiazole based wide bandgap donor polymers enable 19.54% efficiency organic solar cells along with desirable batch-to-batch reproducibility and general applicability *Adv. Mater.* **35** 2300631
[9] Peng J, Wang K, Li M, Peng Z, Liu H, Huang M and Zhao B A-A strategy enables desirable performance of all-polymer solar cells fabricated with nonhalogenated solvents *ACS Appl. Mater. Interfaces* **15** 48255–63
[10] Deng M, Xu X, Duan Y, Yu L, Li R and Peng Q 2023 Y-type non-fullerene acceptors with outer branched side chains and inner cyclohexane side chains for 19.36% efficiency polymer solar cells *Adv. Mater.* **35** 2210760
[11] Zhan L *et al* 2022 Manipulating charge transfer and transport via intermediary electron acceptor channels enables 19.3% efficiency organic photovoltaics *Adv. Energy Mater.* **12** 2201076
[12] He C *et al* 2022 Manipulating the D A interfacial energetics and intermolecular packing for 19.2% efficiency organic photovoltaics *Energy Environ. Sci.* **15** 2537–44
[13] Guo C *et al* 2023 A polycrystalline polymer donor as pre-aggregate toward ordered molecular aggregation for 19.3% efficiency binary organic solar cells *Adv. Mater.* **35** 2304921
[14] Gao J *et al* 2022 Over 19.2% efficiency of organic solar cells enabled by precisely tuning the charge transfer state via donor alloy strategy *Adv. Sci.* **9** 2203606
[15] Wang J *et al* 2023 Binary organic solar cells with 19.2% efficiency enabled by solid additive *Adv. Mater.* **35** 2301583
[16] Chen H, Zhang Z-G and Gao F 2023 Solidification of solvent additive for stable binary polymer solar cells with ∼19% efficiency *Sci. China Mater.* **66** 2523–4
[17] Würfel U, Herterich J, List M, Faisst J, Bhuyian M F M, Schleiermacher H F, Knupfer K T and Zimmermann B 2021 A 1 cm2 organic solar cell with 15.2% certified efficiency detailed characterization and identification of optimization potential *Solar RRL* **5** 2000802
[18] Faisst J, Jiang E, Bogati S, Pap L, Zimmermann B, Kroyer T, Würfel U and List M 2023 Organic solar cell with an active area > 1 cm^2 achieving 15.8% certified efficiency using optimized VIS-NIR antireflection coating *Solar RRL* **7** 2300663
[19] Distler A, Brabec C J and Egelhaaf H-J 2021 Organic photovoltaic modules with new world record efficiencies *Prog. Photovolt.: Res. Appl.* **29** 24–31
[20] Basu R, Gumpert F, Lohbreier J, Morin P O, Vohra V, Liu Y and Distler A 2024 Large-area organic photovoltaic modules with 14.5% certified world record efficiency *Joule* **8** 970–8
[21] Berny S *et al* 2016 Solar trees first large-scale demonstration of fully solution coated, semitransparent, flexible organic photovoltaic modules *Adv. Sci.* **3** 1500342
[22] Brabec C J and Durrant J R 2008 Solution-processed organic solar cells *MRS Bull.* **33** 670–5
[23] Jiang Y *et al* 2022 An alcohol-dispersed conducting polymer complex for fully printable organic solar cells with improved stability *Nat. Energy* **7** 352–9
[24] Ma Z, Zhao B, Gao H, Gong Y, Yu R and Tan Z 2022 Recent advances of crosslinkable organic semiconductors in achieving solution-processed and stable optoelectronic devices *J. Mater. Chem.* A **10** 18542–76
[25] Peng Z, Stingelin N, Ade H and Michels J J 2023 A materials physics perspective on structure-processing-function relations in blends of organic semiconductors *Nat. Rev. Mater.* **8** 439–55

[26] Zhu L et al 2021 Progress and prospects of the morphology of non-fullerene acceptor based high-efficiency organic solar cells *Energy Environ. Sci.* **14** 4341–57
[27] Zhang Y, Lang Y and Li G 2023 Recent advances of non-fullerene organic solar cells From materials and morphology to devices and applications *EcoMat* **5** e12281
[28] Peng Z, Ye L and Ade H 2022 Understanding, quantifying, and controlling the molecular ordering of semiconducting polymers from novices to experts and amorphous to perfect crystals *Mater. Horiz.* **9** 577–606
[29] Tam K C, Saito H, Maisch P, Forberich K, Feroze S, Hisaeda Y, Brabec C J and Egelhaaf H-J 2022 Highly reflective and low resistive top electrode for organic solar cells and modules by low temperature silver nanoparticle ink *Solar RRL* **6** 2100887
[30] Maisch P, Tam K C, Lucera L, Egelhaaf H-J, Scheiber H, Maier E and Brabec C J 2016 Inkjet printed silver nanowire percolation networks as electrodes for highly efficient semitransparent organic solar cells *Organ. Electron.* **38** 139–43
[31] Guo F, Li N, Radmilović V, . Radmilović V R, Turbiez V, Spiecker M E, Forberich K and Brabec C J 2015 Fully printed organic tandem solar cells using solution-processed silver nanowires and opaque silver as charge collecting electrodes *Energy Environ. Sci.* **8** 1690–7
[32] Tam K C, Kubis P, Maisch P, Brabec C J and Egelhaaf H-J 2022 Fully printed organic solar modules with bottom and top silver nanowire electrodes *Prog. Photovolt.: Res. Appl.* **30** 528–42
[33] Booth R E, Schrickx H M, Hanby G, Liu Y, Qin Y, Ade H, Zhu Y and O'Connor B T 2022 Silver nanowire composite electrode enabling highly flexible, robust organic photovoltaics *Solar RRL* **6** 2200264
[34] Murad A R, Iraqi A, Aziz A, Abdullah S N and Brza M A 2020 Conducting polymers for optoelectronic devices and organic solar cells a review *Polymers* **12** 2627
[35] Alemu D, Wei H-Y, Ho K-C and Chu C-W 2012 Highly conductive PEDOT PSS electrode by simple film treatment with methanol for ITO-free polymer solar cells *Energy Environ. Sci.* **5** 9662–71
[36] Xie C, Liu Y, Wei W and Zhou Y 2023 Large-Area Flexible Organic Solar Cells with a Robust Silver Nanowire-Polymer Composite as Transparent Top Electrode *Adv. Funct. Mater.* **33** 2210675
[37] Ahsan Saeed M, Hyeon Kim S, Baek K, Hyun J K, Youn Lee S and Won Shim J 2021 PEDOT PSS CuNW-based transparent composite electrodes for high-performance and flexible organic photovoltaics under indoor lighting *Appl. Surf. Sci.* **30** 567150852
[38] Zhu Y, Deng Y, Yi P, Peng L, Lai X and Lin Z 2019 Flexible transparent electrodes based on silver nanowires material synthesis, fabrication, performance, and applications *Adv. Mater. Technol.* **4** 1900413
[39] Verboven I, Silvano J, Elen K, Pellaers H, Ruttens B, D'Haen J, Van Bael M K, Hardy A and Deferme W 2022 Ultrasonic spray coating of silver nanowire-based electrodes for organic light-emitting diodes *Adv. Eng. Mater.* **24** 2100808
[40] Lucera L, Kubis P, Fecher F W, Bronnbauer C, Turbiez M, Forberich K, Ameri T, Egelhaaf H-J and Brabec C J 2015 Guidelines for closing the efficiency gap between hero solar cells and roll-to-roll printed modules *Energy Technol.* **3** 373–84
[41] Kant C, Shukla A, McGregor S K M, Lo S C, Namdas E B and Katiyar M 2023 Large area inkjet-printed OLED fabrication with solution-processed TADF ink *Nat. Commun.* **14** 7220
[42] Cinquino M 2024 Toward highly efficient solution-processable OLEDs inkjet printing of TADF emissive layer *Adv. Electron. Mater.* **10** 2300358
[43] Chennit K et al 2023 Inkjet-printed, coplanar electrolyte-gated organic field-effect transistors on flexible substrates fabrication, modeling, and applications in biodetection *Adv. Mater. Technol.* **8** 2200300
[44] Liu Y, Yang C, Jiang T, Bao Y, Wang L, Ji D, Yang F, Jiao F and Hu W 2023 A C 6 -DPA/PMMA binary blend ink for high-performance inkjet-printed organic field-effect transistors *Mater. Adv.* **4** 302–6
[45] Maisch P 2019 Process development for inkjet printing of organic photovoltaics *Doctoral dissertation* Friedrich-Alexander-Universität Erlangen-Nürnberg (FAU)
[46] Bihar E, Corzo D, Hidalgo T C, Rosas-Villalva D, Salama K N, Inal S and Baran D Fully inkjet-printed, ultrathin and conformable organic photovoltaics as power source based on cross-linked PEDOT PSS electrodes *Adv. Mater. Technol.* **5** 2000226
[47] Maisch P, Tam K C, Jang D, Steinberger M, Yang F, Brabec C J and Egelhaaf H J 2021 Inkjet printed organic and perovskite photovoltaics-review and perspectives *npj Flex. Electron.* 305–33
[48] Chen X Z, Luo Q and Ma C Q 2023 Inkjet-printed organic solar cells and perovskite solar cells progress, challenges, and prospect *Chin. J. Polym. Sci.* **41** 1169–97
[49] Bastola A et al 2023 Formulation of functional materials for inkjet printing A pathway towards fully 3D printed electronics *Mater. Today Electron.* **6** 100058
[50] Xia Z, Cai T, Li X, Zhang Q, Shuai J and Liu S 2023 Recent progress of printing technologies for high-efficient organic solar cells *Catalysts* **13** 156
[51] Lohse D 2022 Fundamental fluid dynamics challenges in inkjet printing *Annu. Rev. Fluid Mech.* **54** 349–82
[52] Sang L et al 2023 Elimination of drying-dependent component deviation using a composite solvent strategy enables high-performance inkjet-printed organic solar cells with efficiency approaching 16% *Adv. Funct. Mater.* **33** 2304824
[53] Corzo D, Bihar E, Alexandre E B, Rosas-Villalva D and Baran D 2011 Ink engineering of transport layers for 9.5% efficient all-printed semitransparent nonfullerene solar cells *Adv. Funct. Mater.* **31** 2005763
[54] Kang M H, Heo D K, Kim D H, Lee M, Ryu K, Kim Y H and Yun C 2019 Fabrication of spray-coated semitransparent organic solar cells *IEEE J. Electron. Devices Soc.* **7** 1129–32
[55] Park S Y, Kang Y J, Lee S, Kim D G, Kim J K, Kim J H and Kang J-W 2011 Spray-coated organic solar cells with large-area of 12.25cm2 *Sol. Energy Mater. Sol. Cells* **95** 852–5
[56] Steirer K X, Reese M O, Rupert B L, Kopidakis N, Olson D C, Collins R T and Ginley D S 2009 Ultrasonic spray deposition for production of organic solar cells *Sol. Energy Mater. Sol. Cells* **93** 447–53
[57] Lewis J E, Lafalce E, Toglia P and Jiang X 2011 Over 30% transparency large area inverted organic solar array by spray *Sol. Energy Mater. Sol. Cells* **95** 2816–22
[58] Susanna G, Salamandra L, Brown T M, Di Carlo A, Brunetti F and Reale A 2011 Airbrush spray-coating of polymer bulk-heterojunction solar cells *Sol. Energy Mater. Sol. Cells* **95** 1775–8
[59] Girotto C, Moia D, Rand B P and Heremans P 2011 High-performance organic solar cells with spray-coated hole-transport and active layers *Adv. Funct. Mater.* **21** 64–72
[60] Aziz F and Ismail A F 2015 Spray coating methods for polymer solar cells fabrication A review *Mater. Sci. Semicond. Process.* **39** 416–25
[61] Krebs F C 2009 Fabrication and processing of polymer solar cells A review of printing and coating techniques *Sol. Energy Mater. Sol. Cells* **93** 394–412
[62] Lee J-H, Sagawa T and Yoshikawa S 2011 Morphological and topographical characterizations in spray coated organic solar cells using an additional solvent spray deposition *Organ. Electron.* **12** 2165–73
[63] Colella S, Mazzeo M, Melcarne G, Carallo S, Ciccarella G and Gigli G 2013 Spray coating fabrication of organic solar

cells bypassing the limit of orthogonal solvents *Appl. Phys. Lett.* **102**
[64] Zhao H *et al* 2020 Hot hydrocarbon-solvent slot-die coating enables high-efficiency organic solar cells with temperature-dependent aggregation behavior *Adv. Mater.* **32** 2002302
[65] Goth C, Putzo S and Franke J 2011 Aerosol Jet printing on rapid prototyping materials for fine pitch electronic applications *2011 IEEE 61st Electronic Components and Technology Conf. (ECTC)* pp 1211–6 (available at: https://ieeexplore.ieee.org/abstract/document/5898664 (Accessed 20 December 2023)
[66] Yang P, Zhai T, Yu B, Du G, Mi B, Zhao X and Deng W 2021 Toward all aerosol printing of high-efficiency organic solar cells using environmentally friendly solvents in ambient air *J. Mater. Chem.* A **9** 17198–210
[67] Basu R, Siah K S, Distler A, Häußler F, Franke J, Brabec C J and Egelhaaf H-J 2023 Aerosol-jet-printed encapsulation of organic photovoltaics *Adv. Eng. Mater.* **25** 2300322
[68] Steinberger M, Distler A, Hörber J, Tam K C, Brabec C J and Egelhaaf H J 2024 All inkjet-printed organic solar cells on 3D objects *Flex. Print. Electron.* **9** 025018
[69] Kwon K S, Rahman M K, Phung T H, Hoath S D, Jeong S and Kim J S 2020 Review of digital printing technologies for electronic materials *Flex. Print. Electron.* **5** 043003
[70] Shah V and Wallace D B 2004 Low-cost solar cell fabrication by drop-on-demand ink-jet printing *Proc. MAPS 37th Annual Int. Symp. on Microelectronics*
[71] Hoth C N, Choulis S A, Schilinsky P and Brabec C J 2007 High photovoltaic performance of inkjet printed polymer fullerene blends *Adv. Mater.* **19** 3973–8
[72] Hoth C N, Schilinsky P, Choulis S A and Brabec C J 2008 Printing highly efficient organic solar cells *Nano Lett.* **8** 2806–13
[73] Eom S H, Senthilarasu S, Uthirakumar P, Yoon S C, Lim J, Lee C, Lim H S, Lee J and Lee S-H 2009 Polymer solar cells based on inkjet-printed PEDOT PSS layer *Organ. Electron.* **10** 536–42
[74] Lange A, Wegener M, Boeffel C, Fischer B, Wedel A and Neher D 2010 A new approach to the solvent system for inkjet-printed P3HT PCBM solar cells and its use in devices with printed passive and active layers *Sol. Energy Mater. Sol. Cells* **94** 1816–21
[75] Eom S H, Park H, Mujawar S H, Yoon S C, Kim S S, Na S I, Kang S-J, Khim D, Kim D-Y and Lee S-H 2010 High efficiency polymer solar cells via sequential inkjet-printing of PEDOT PSS and P3HT PCBM inks with additives *Organ. Electron.* **11** 1516–22
[76] Jeong J A, Lee J, Kim H, Kim H K and Na S I 2010 Ink-jet printed transparent electrode using nano-size indium tin oxide particles for organic photovoltaics *Sol. Energy Mater. Sol. Cells* **94** 1840–4
[77] Teichler A, Eckardt R, Hoeppener S, Friebe C, Perelaer J, Senes A, Morana M, Brabec C J and Schubert U S 2011 Combinatorial screening of polymer: fullerene blends for organic solar cells by inkjet printing *Adv. Energy Mater.* **1** 105–14
[78] Galagan Y, Coenen E W C, Sabik S, Gorter H H, Barink M, Veenstra S C, Kroon J M, Andriessen R and Blom P W 2012 Evaluation of ink-jet printed current collecting grids and busbars for ITO-free organic solar cells *Sol. Energy Mater. Sol. Cells* **104** 32–8
[79] Angmo D, Sweelssen J, Andriessen R, Galagan Y and Krebs F C 2013 Inkjet printing of back electrodes for inverted polymer solar cells *Adv. Energy Mater.* **3** 1230–7
[80] Lange A, Schindler W, Wegener M, Fostiropoulos K and Janietz S 2013 Inkjet printed solar cell active layers prepared from chlorine-free solvent systems *Sol. Energy Mater. Sol. Cells* **109** 104–10
[81] Jung S, Sou A, Banger K, Ko D H, Chow P C Y, McNeill C R and Sirringhaus H 2014 All-inkjet-printed, all-air-processed solar cells *Adv. Energy Mater.* **4** 1400432
[82] Lu H, Lin J, Wu N, Nie S, Luo Q, Ma C Q and Cui Z 2015 Inkjet printed silver nanowire network as top electrode for semi-transparent organic photovoltaic devices *Appl. Phys. Lett.* **106** 093302
[83] Eggenhuisen T M, Galagan Y, Coenen E W C, Voorthuijzen W P, Slaats M W L, Kommeren S A, Shanmuganam S, Coenen M J, Andriessen R and Groen WA 2015 Digital fabrication of organic solar cells by Inkjet printing using non-halogenated solvents *Sol. Energy Mater. Sol. Cells* **134** 364–72
[84] Eggenhuisen T M *et al* 2015 High efficiency, fully inkjet printed organic solar cells with freedom of design *J. Mater. Chem.* A **3** 7255–62
[85] Sankaran S, Glaser K, Gaertner S, Roedlmeier T, Sudau K, Hernandez-Sosa G and Colsmann A 2016 Fabrication of polymer solar cells from organic nanoparticle dispersions by doctor blading or ink-jet printing *Organ. Electron.* **28** 118–22
[86] Kommeren S, Coenen M J J, Eggenhuisen T M, Slaats T W L, Gorter H and Groen P 2018 Combining solvents and surfactants for inkjet printing PEDOT PSS on P3HT/PCBM in organic solar cells *Organ. Electron.* **61** 282–8
[87] Kastner J, Gnatiuk I, Wagner M, Holzinger D, Rudelstorfer V, Hesser G, Fuchsbauer A and Hild S 2019 Grinded nano-graphite inkjet inks for application in organic solar cells *Nanotechnology* **30** 04601
[88] Corzo D, Almasabi K, Bihar E, Macphee S, Rosas-villalva D, Gasparini N, Inal S and Baran D 2019 Digital inkjet printing of high-efficiency large-area nonfullerene organic solar cells *Adv. Mater. Technol.* **4** 1900040
[89] Lan S, Zhong J and Wang X Impact of inkjet printing parameters on the morphology and device performance of organic photovoltaics *J. Appl. Phys.* **54** 465105
[90] Perkhun P *et al* 2021 High-efficiency digital inkjet-printed non-fullerene polymer blends using non-halogenated solvents *Adv. Energy Sustain. Res.* **2** 2000086
[91] Chen X, Huang R, Han Y, Zha W, Fang J, Lin J, Luo Q, Chen Z and Ma C-Q 2022 Balancing the molecular aggregation and vertical phase separation in the polymer nonfullerene blend films enables 13.09% efficiency of organic solar cells with inkjet-printed active layer *Adv. Energy Mater.* **12** 2200044
[92] Kastner J, Tomarchio F, Decorde N, Kehrer M, Hesser G and Fuchsbauer A 2023 Integration of inkjet printed graphene as a hole transport layer in organic solar cells *Micromachines* **14** 1858
[93] Hoath S D ed 2016 *Fundamentals of Inkjet Printing the Science of Inkjet and Droplets* 1st edn (Wiley) (https://doi.org/10.1002/9783527684724) (Accessed 20 December 2023)
[94] Wijshoff H 2010 The dynamics of the piezo inkjet printhead operation *Phys. Rep.* **491** 77–177
[95] Kang S H, Kim S, Sohn D K and Ko H S 2020 Analysis of drop-on-demand piezo inkjet performance *Phys. Fluids* **32** 022007
[96] Noguera R, Lejeune M and Chartier T 2005 3D fine scale ceramic components formed by ink-jet prototyping process *J. Eur. Ceram. Soc.* **25** 2055–9
[97] Eggenhuisen T M, Galagan Y, Biezemans A, Coenen M, Gilot J, Groen P and Andriessen R 2014 Organic photovoltaic cells with all inkjet printed layers and freedom of form *2014 IEEE 40th Photovoltaic Specialist Conf., PVSC* pp 2842–5
[98] Wadsworth A, Hamid Z, Kosco J, Gasparini N and McCulloch I 2020 The bulk heterojunction in organic photovoltaic, photodetector, and photocatalytic applications *Adv. Mater.* **32** 2001763
[99] Treat N D, Westacott P and Stingelin N 2015 The power of materials science tools for gaining insights into organic semiconductors *Annu. Rev. Mater. Res.* **45** 459–90

[100] Ronsin O J J and Harting J 2022 Phase-field simulations of the morphology formation in evaporating crystalline multicomponent films *Adv. Theor. Simul.* **5** 2200286
[101] Schmidt-Hansberg B *et al* 2011 Moving through the phase diagram morphology formation in solution cast polymer-fullerene blend films for organic solar cells *ACS Nano* **5** 8579–90
[102] Ulum S, Holmes N, Barr M, Kilcoyne A L D, Gong B B, Zhou X, Belcher W and Dastoor P 2013 The role of miscibility in polymer fullerene nanoparticulate organic photovoltaic devices *Nano Energy* **2** 897–905
[103] Ye L *et al* 2018 Quantitative relations between interaction parameter, miscibility and function in organic solar cells *Nat. Mater.* **17** 253–60
[104] Li N, Machui F, Waller D, Koppe M and Brabec C J 2011 Determination of phase diagrams of binary and ternary organic semiconductor blends for organic photovoltaic devices *Sol. Energy Mater. Sol. Cells* **95** 3465–71
[105] Ye L, Collins B A, Jiao X, Zhao J, Yan H and Ade H 2018 Miscibility-function relations in organic solar cells significance of optimal miscibility in relation to percolation *Adv. Energy Mater.* **8** 1703058
[106] Levitsky A *et al* 2020 Toward fast screening of organic solar cell blends *Adv. Sci.* **7** 2000960
[107] Levitsky A, Schneider S A, Rabkin E, Toney M F and Frey G L 2021 Bridging the thermodynamics and kinetics of temperature-induced morphology evolution in polymer/fullerene organic solar cell bulk heterojunction *Mater. Horiz.* **8** 1272–85
[108] Saller C, Kahle F J, Müller T, Hahn T, Tscheuschner S, Priadko D, Strohriegl P, Bässler H and Köhler A Facile method for the investigation of temperature-dependent C_{60} diffusion in conjugated polymers *ACS Appl. Mater. Interfaces* **10** 21499–509
[109] Ye L, Li S, Liu X, Zhang S, Ghasemi M, Xiong Y, Hou J and Ade H 2019 Quenching to the percolation threshold in organic solar cells *Joule* **3** 443–58
[110] Ghasemi M *et al* 2021 A molecular interaction-diffusion framework for predicting organic solar cell stability *Nat. Mater.* **20** 525–32
[111] Lee C K and Pao C W 2016 Multiscale molecular simulation of solution processing of SMDPPEH PCBM small-molecule organic solar cells *ACS Appl. Mater. Interfaces* **8** 20691–700
[112] Du C, Ji Y, Xue J, Hou T, Tang J, Lee S T and Li Y 2015 Morphology and performance of polymer solar cell characterized by DPD simulation and graph theory *Sci. Rep.* **5**
[113] Ray B, Nair P R and Alam M A 2011 Annealing dependent performance of organic bulk-heterojunction solar cells A theoretical perspective *Sol. Energy Mater. Sol. Cells* **95** 3287–94
[114] Alam M A, Ray B, Khan M R and Dongaonkar S 2013 The essence and efficiency limits of bulk-heterostructure organic solar cells A polymer-to-panel perspective *J. Mater. Res.* **28** 541–57
[115] Gebhardt R S, Du P, Wodo O and Ganapathysubramanian B 2017 A data-driven identification of morphological features influencing the fill factor and efficiency of organic photovoltaic devices *Comput. Mater. Sci* **129** 220–5
[116] Kaka F, Singh R K, Ramamurthy P C and Choudhury A 2020 Modeling process-structure-property relationship in organic photovoltaics using a robust diffuse interface approach *AIP Adv.* **10** 065304
[117] Kaka F, Khanna S, Ramamurthy P C and Choudhury A 2020 Investigation of process-structure-property relationship in ternary organic photovoltaics *J. Appl. Phys.* **128** 145501
[118] Bergermann K, Deibel C, Herzog R, MacKenzie R C I, Null J F P and Stoll M 2023 Preconditioning for a phase-field model with application to morphology evolution in organic semiconductors *CiCP* **34** 1–17
[119] Michels J J and Moons E Simulation of surface-directed phase separation in a solution-processed polymer/PCBM blend *Macromolecules* **46** 8693–701
[120] Kouijzer S, Michels J J, van den Berg M, Gevaerts V S, Turbiez M, Wienk M M and Janssen R A J 2013 Predicting morphologies of solution processed polymer fullerene blends *J. Am. Chem. Soc.* **135** 12057–67
[121] Wodo O and Ganapathysubramanian B 2012 Modeling morphology evolution during solvent-based fabrication of organic solar cells *Comput. Mater. Sci* **55** 113–26
[122] Wodo O and Ganapathysubramanian B 2014 How do evaporating thin films evolve? Unravelling phase-separation mechanisms during solvent-based fabrication of polymer blends *Appl. Phys. Lett.* **105** 153104
[123] Negi V, Wodo O, van Franeker J J, Janssen R A J and Bobbert P A 2018 Simulating phase separation during spin coating of a polymer-fullerene blend a joint computational and experimental investigation *ACS Appl. Energy Mater.* **1** 725–35
[124] Michels J J, Zhang K, Wucher P, Beaujuge P M, Pisula W and Marszalek T 2021 Predictive modelling of structure formation in semiconductor films produced by meniscus-guided coating *Nat. Mater.* **20** 68–75
[125] Ronsin O J J, Jang D, Egelhaaf H J, Brabec C J and Harting J Phase-field simulation of liquid-vapor equilibrium and evaporation of fluid mixtures *ACS Appl. Mater. Interfaces* **13** 55988–6003
[126] Ronsin O J J and Harting J 2022 Formation of crystalline bulk heterojunctions in organic solar cells insights from phase-field simulations *ACS Appl. Mater. Interfaces* **14** 49785–800
[127] Ruderer M A, Guo S, Meier R, Chiang H Y, Körstgens V, Wiedersich J, Perlich J, Roth S V and Müller-Buschbaum P 2011 Solvent-induced morphology in polymer-based systems for organic photovoltaics *Adv. Funct. Mater.* **21** 3382–91
[128] Yao G, Ge Y, Xiao X, Zhang L, Yi N, Luo H, Yuan S and Zhou W 2022 Preaggregation in solution producing multiple crystal forms of Y6 corresponding to a variation of miscibility in PM6-Based ternary solar cells *ACS Appl. Energy Mater.* **5** 1193–204
[129] Schaefer C, Michels J J and van der Schoot P 2016 Structuring of thin-film polymer mixtures upon solvent evaporation *Macromolecules* **49** 6858–70
[130] Zhou Z, Xu S, Song J, Jin Y, Yue Q, Qian Y, Liu F, Zhang F and Zhu X 2018 High-efficiency small-molecule ternary solar cells with a hierarchical morphology enabled by synergizing fullerene and non-fullerene acceptors *Nat. Energy* **3** 952–9
[131] Zeng R *et al* All-polymer organic solar cells with nano-to-micron hierarchical morphology and large light receiving angle *Nat. Commun.* **14** 4148
[132] McDowell C, Abdelsamie M, Toney M F and Bazan G C 2018 Solvent additives key morphology-directing agents for solution-processed organic solar cells *Adv. Mater.* **30** 1707114
[133] Ganesan S, Gollu S R, Alam Khan J, Kushwaha A and Gupta D 2019 Inkjet printing of zinc oxide and P3HT ICBA in ambient conditions for inverted bulk heterojunction solar cells *Opt. Mater.* **94** 430–5
[134] Singh A, Gupta S K and Garg A 2016 Inverted polymer bulk heterojunction solar cells with ink-jet printed electron transport and active layers *Organ. Electron.* **35** 118–27
[135] Singh A, Gupta S K and Garg A 2017 Inkjet printing of NiO films and integration as hole transporting layers in polymer solar cells *Sci. Rep.* **7** 1775
[136] Ganesan S and Gupta D 2020 Fabrication of indium tin oxide free bulk heterojunction organic solar cells using inkjet-printed silver grids and PEDOT PSS *Mater. Res. Express* **6** 125120

[137] Maisch P, Eisenhofer L M, Tam K C, Distler A, Voigt M M, Brabec C J and Egelhaaf H J 2019 A generic surfactant-free approach to overcome wetting limitations and its application to improve inkjet-printed P3HT non-fullerene acceptor PV *J. Mater. Chem.* A **7** 13215–24
[138] Cazabat A M and Guéna G 2010 Evaporation of macroscopic sessile droplets *Soft Matter* **6** 2591–612
[139] Stauber J, Wilson S, Duffy B and Sefiane K 2014 On the lifetimes of evaporating droplets *J. Fluid Mech.* **31** 744
[140] Picknett R G and Bexon R 1977 The evaporation of sessile or pendant drops in still air *J. Colloid Interface Sci.* **61** 336–50
[141] Gelderblom H 2013 Fluid flow in drying drops (available at: https://research.utwente.nl/en/publications/fluid-flow-in-drying-drops) (Accessed 30 January 2024)
[142] Deegan R D, Bakajin O, Dupont T F, Huber G, Nagel S R and Witten T A 1997 Capillary flow as the cause of ring stains from dried liquid drops *Nature* **389** 827–9
[143] Hu H and Larson R G Evaporation of a sessile droplet on a substrate *J. Phys. Chem.* B **106** 1334–44
[144] Popov Y O 2005 Evaporative deposition patterns spatial dimensions of the deposit *Phys. Rev.* E **71** 036313
[145] Gelderblom H, Marín Á G, Nair H, van Houselt A, Lefferts L, Snoeijer J H and Lohse D 2011 How water droplets evaporate on a superhydrophobic substrate *Phys. Rev.* E **83** 026306
[146] Yunker P J, Still T, Lohr M A and Yodh A G 2011 Suppression of the coffee-ring effect by shape-dependent capillary interactions *Nature* **476** 308–11
[147] Yunker P J, Lohr M A, Still T, Borodin A, Durian D J and Yodh A G 2013 Effects of particle shape on growth dynamics at edges of evaporating drops of colloidal suspensions *Phys. Rev. Lett.* **110** 035501
[148] Dugyala V R and Basavaraj M G 2016 Control over coffee-ring formation in evaporating liquid drops containing ellipsoids *Langmuir* **30** 8680–6
[149] Kim D-O, Pack M, Hu H, Kim H and Sun Y 2016Deposition of colloidal drops containing ellipsoidal particles competition between capillary and hydrodynamic forces *Langmuir* **32** 11899–906
[150] Sangani A S, Lu C, Su K and Schwarz J A 2009 Capillary force on particles near a drop edge resting on a substrate and a criterion for contact line pinning *Phys. Rev.* E **80** 011603
[151] Weon B M and Je J H 2010 Capillary force repels coffee-ring effect *Phys. Rev.* E **82** 015305
[152] Perelaer J, Smith P J, Hendriks C E, Amj V D B and Schubert U S 2008 The preferential deposition of silica micro-particles at the boundary of inkjet printed droplets *Soft Matter* **4** 1072–8
[153] Bhardwaj R, Fang X, Somasundaran P and Attinger D 2010 Self-assembly of colloidal particles from evaporating droplets role of DLVO interactions and proposition of a phase diagram *Langmuir* **26** 7833–42
[154] Bigioni T P, Lin X-M, Nguyen T T, Corwin E I, Witten T A and Jaeger H M 2006 Kinetically driven self assembly of highly ordered nanoparticle monolayers *Nat. Mater.* **5** 265–70
[155] Anyfantakis M, Geng Z, Morel M, Rudiuk S and Baigl D 2015 Modulation of the coffee-ring effect in particle/surfactant mixtures the importance of particle-interface interactions *Langmuir* **31** 4113–20
[156] van Gaalen R T, Diddens C, Wijshoff H M A and Kuerten J G M 2021 Marangoni circulation in evaporating droplets in the presence of soluble surfactants *J. Colloid Interface Sci.* **15** 584622–33
[157] Li Y-F, Sheng Y-J and Tsao H-K 2013 Evaporation stains suppressing the coffee-ring effect by contact angle hysteresis *Langmuir* **29** 7802–11
[158] Hu H and Larson R G 2005 Analysis of the effects of marangoni stresses on the microflow in an evaporating sessile droplet *Langmuir* **21** 3972–80
[159] Lohse D and Zhang X 2015 Surface nanobubbles and nanodroplets *Rev. Mod. Phys.* **87** 981–1035
[160] Fleck N A, McMeeking R M and Kraus T 2015 Convective assembly of a particle monolayer *Langmuir* **31** 13655–63
[161] Pham T and Kumar S 2017 Drying of droplets of colloidal suspensions on rough substrates *Langmuir* **33** 10061–76
[162] Hessling D, Xie Q and Harting J 2017 Diffusion dominated evaporation in multicomponent lattice Boltzmann simulations *J. Chem. Phys.* **146** 054111
[163] Xie Q and Harting J 2018 From dot to ring the role of friction in the deposition pattern of a drying colloidal suspension droplet *Langmuir* **34** 5303–11
[164] van Dam D B and Kuerten J G M 2008 Modeling the drying of ink-jet-printed structures and experimental verification *Langmuir* **24** 582–9
[165] Siregar D P, Kuerten J G M and van der Geld C W M 2013 Numerical simulation of the drying of inkjet-printed droplets *J. Colloid Interface Sci.* **15** 392388–95
[166] van Gaalen R T, Diddens C, Wijshoff H M A and Kuerten J G M 2020 The evaporation of surfactant-laden droplets A comparison between contact line models *J. Colloid Interface Sci.* **579** 579888–97
[167] Diddens C 2017 Detailed finite element method modeling of evaporating multi-component droplets *J. Comput. Phys.* **340** 670–87
[168] Davies G B, Krüger T, Coveney P V, Harting J and Bresme F 2014 Assembling ellipsoidal particles at fluid interfaces using switchable dipolar capillary interactions *Adv. Mater.* **26** 6715–9
[169] Wouters M, Aouane O, Sega M and Harting J 2021 Lattice Boltzmann simulations of drying suspensions of soft particles *Phil. Trans. R. Soc.* A **379** 20200399
[170] Pelusi F, Guglietta F, Sega M, Aouane O and Harting J A sharp interface approach for wetting dynamics of coated droplets and soft particles *Phys. Fluids* **35** 082126
[171] Hu H and Larson R G 2006 Marangoni Effect Reverses Coffee-Ring Depositions *J. Phys. Chem.* A **110** 7090–4
[172] Soltman D and Subramanian V 2008 Inkjet-printed line morphologies and temperature control of the coffee ring effect *Langmuir* **24** 2224–31
[173] Cherian D, Mitra K Y, Hartwig M, Malinowski P E and Baumann R R 2018 Fabrication of organic photo detectors using inkjet technology and its comparison to conventional deposition processes *IEEE Sens. J.* **18** 94–105
[174] Soltman D B 2024 Understanding inkjet printed pattern generation *PhD* Ann Arbor, United States (available at:www.proquest.com/docview/1440475417/abstract/C1E5F8D5634244B3PQ/1)
[175] Du Z, Zhou H, Yu X and Han Y 2020 Controlling the polarity and viscosity of small molecule ink to suppress the contact line receding and coffee ring effect during inkjet printing *Colloids Surf.* A **602** 125111
[176] Al-Milaji K N, Secondo R R, Ng T N, Kinsey N and Zhao H 2018 Interfacial self-assembly of colloidal nanoparticles in dual-droplet inkjet printing *Adv. Mater. Interfaces* **5** 1701561
[177] Kuang M, Wang L and Song Y 2014 Controllable printing droplets for high-resolution patterns *Adv. Mater.* **26** 6950–8
[178] Matavž A, Frunză R C, Drnovšek A, Bobnar V and Malič B 2016 Inkjet printing of uniform dielectric oxide structures from sol-gel inks by adjusting the solvent composition *J. Mater. Chem.* C **4** 5634–41
[179] Pan Y, Liu H, Wang S, Han X and Li X 2021 Inkjet-printed alloy-like cross-linked hole-transport layer for high-performance solution-processed green phosphorescent OLEDs *J. Mater. Chem.* C **9** 12712–9
[180] Lim J A, Lee W H, Lee H S, Lee J H, Park Y D and Cho K 2008 Self-organization of ink-jet-printed triisopropylsilylethynyl pentacene via evaporation-induced flows in a drying droplet *Adv. Funct. Mater.* **18** 229–34
[181] He P and Derby B 2017 Controlling coffee ring formation during drying of inkjet printed 2D inks *Adv. Mater. Interfaces* **4** 1700944

[182] Huang Y C, Cha H C, Chen C Y and Tsao C S 2016 Morphological control and performance improvement of organic photovoltaic layer of roll-to-roll coated polymer solar cells *Sol. Energy Mater. Sol. Cells* **150** 10–8
[183] Du X, Heumueller T, Gruber W, Classen A, Unruh T, Li N and Brabec C J 2019 Efficient polymer solar cells based on non-fullerene acceptors with potential device lifetime approaching 10 years *Joule* **3** 215–26
[184] Channa I A, Shah A A, Rizwan M, Makhdoom M A, Chandio A D, Shar M A and Mahmood A 2021 Process parameter optimization of a polymer derived ceramic coatings for producing ultra-high gas barrier *Materials* **14** 7000
[185] Channa I A, Distler A, Brabec C J and Egelhaaf H J 2021 9-Solution-coated barriers for organic electronics *Organic Flexible Electronics* (*Woodhead Publishing Series in Electronic and Optical Materials)* ed P Cosseddu and M Caironi (Woodhead Publishing) pp 249–303 (available at:www.sciencedirect.com/science/article/pii/B9780128188903000096) (Accessed 30 January 2024)
[186] Channa I A, Chandio A D, Rizwan M, Shah A A, Bhatti J, Shah A K, Hussain F, Shar M A and AlHazaa A 2021 Solution processed PVB/Mica flake coatings for the encapsulation of organic solar cells *Materials* **14** 2496
[187] Maisch P, Tam K C, Schilinsky P, Egelhaaf H-J and Brabec C J 2018 Shy organic photovoltaics digitally printed organic solar modules with hidden interconnects *Solar RRL* **2** 1–9
[188] Angmo D, Larsen-Olsen T T, Jørgensen M, Søndergaard R R and Krebs F C 2013 Roll-to-roll inkjet printing and photonic sintering of electrodes for ITO free polymer solar cell modules and facile product integration *Adv. Energy Mater.* **3** 172–5
[189] Lucera L, Machui F, Kubis P, Schmidt H D, Adams J, Strohm S, Ahmad T, Forberich K, Egelhaaf H-J and Brabec C J 2016 Highly efficient, large area, roll coated flexible and rigid OPV modules with geometric fill factors up to 98.5% processed with commercially available materials *Energy Environ. Sci.* **9** 89–94
[190] Josserand C and Thoroddsen S T 2016 Drop impact on a solid surface *Annu. Rev. Fluid Mech.* **48** 365–91
[191] Stringer J and Derby B 2010 Formation and stability of lines produced by inkjet printing *Langmuir* **26** 10365–72
[192] Crozier M L, Brunton A, Henley S J, Shephard J D, Abbas A, Bowers J W, Kaminski P M and Walls J M 2014 Inkjet and laser hybrid processing for series interconnection of thin film photovoltaics *Mater. Res. Innov.* **18** 509–14
[193] Aernouts T, Aleksandrov T, Girotto C, Genoe J and Poortmans J 2008 Polymer based organic solar cells using ink-jet printed active layers *Appl. Phys. Lett.* **92** 033306
[194] Yu J-S, Kim I, Kim J-S, Jo J, Larsen-Olsen T T, Søndergaard R R, Hösel M, Angmo D, Jørgensen M and Krebs F C 2012 Silver front electrode grids for ITO-free all printed polymer solar cells with embedded and raised topographies, prepared by thermal imprint, flexographic and inkjet roll-to-roll processes *Nanoscale* **4** 6032–40
[195] Fujifilm *Industrial Printheads* (available at: www.fujifilm.com/us/en/business/inkjet-solutions/industrial-printheads) (Accessed 6 February 2024)
[196] Team I. ImageXpert 2021 The ultimate industrialinkjet printhead comparison chart (available at: https://imagexpert.com/the-ultimate-industrial-inkjet-printhead-comparison-chart/) (Accessed 9 May 2024)
[197] Jeong S, Song H C, Lee W W, Choi Y and Ryu B-H 2010 Preparation of aqueous Ag Ink with long-term dispersion stability and its inkjet printing for fabricating conductive tracks on a polyimide film *J. Appl. Phys.* **108** 102805
[198] Steinberger M, Distler A, Brabec C J and Egelhaaf H-J 2022 Improved air processability of organic photovoltaics using a stabilizing antioxidant to prevent thermal oxidation *J. Phys. Chem.* C **126** 22–29
[199] IoT Analytics 2021 *Global IoT spending to grow 24% in 2021, led by investments in IoT software and IoT security* (available at: https://iot-analytics.com/2021-global-iot-spending-grow-24-percent/) (Accessed 30 January 2024)
[200] IoT Analytics 2020 State of the IoT 2020 12 billion IoT connections, surpassing non-IoT for the first time (available at: https://iot-analytics.com/state-of-the-iot-2020-12-billion-iot-connections-surpassing-non-iot-for-the-first-time/) (Accessed 30 January 2024)
[201] Charitatos V, Pham T and Kumar S 2021 Droplet evaporation on inclined substrates *Phys. Rev. Fluids* **6** 084001
[202] Xiang S, Zhang N and Fan X 2021 From fiber to fabric progress towards photovoltaic energy textile *Adv. Fiber Mater.* **3** 76–106
[203] Satharasinghe A, Hughes-Riley T and Dias T 2020 A review of solar energy harvesting electronic textiles *Sensors* **20** 5938
[204] Cui N, Song Y, Tan C H, Zhang K, Yang X, Dong S, Xie B and Huang F 2021 Stretchable transparent electrodes for conformable wearable organic photovoltaic devices *npj Flex. Electron.* **5** 1–8
[205] Qin J, Lan L, Chen S, Huang F, Shi H, Chen W, Xia H, Sun K and Yang C 2020 Recent progress in flexible and stretchable organic solar cells *Adv. Funct. Mater.* **30** 2002529
[206] Dauzon E, Sallenave X, Plesse C, Goubard F, Amassian A and Anthopoulos T D 2021 Pushing the limits of flexibility and stretchability of solar cells a review *Adv. Mater.* **33** 2101469
[207] Lee H, Jeong S, Kim J H, Jo Y R, Eun H J, Park B, Yoon S C, Kim J H, Lee S H and Park S 2023 Ultra-flexible semitransparent organic photovoltaics *npj Flex. Electron.* **7** 1–9
[208] Baran D, Corzo D and Blazquez G 2020 Flexible electronics status, challenges and opportunities *Front. Electron.* **1** 594003
[209] Eid A, Hester J, Fang Y, Tehrani B, Nauroze S A, Bahr R and Tentzeris M M 2019 Nanotechnology-empowered flexible printed wireless electronics a review of various applications of printed materials *IEEE Nanotechnol. Mag.* **13** 18–29
[210] Lüer L, Peters I M, Corre V M L, Forberich K, Guldi D M and Brabec C J 2023 Bypassing the single junction limit with advanced photovoltaic architectures *Adv. Mater.* **36** 2308578